Environmental Science Nano

Accepted Manuscript

This article can be cited before page numbers have been issued, to do this please use: A. Rodd, C. J. Castilho, C. E. Chaparro, J. R. Rangel Mendez, R. Hurt and A. Kane, *Environ. Sci.: Nano*, 2018, DOI: 10.1039/C8EN00352A.

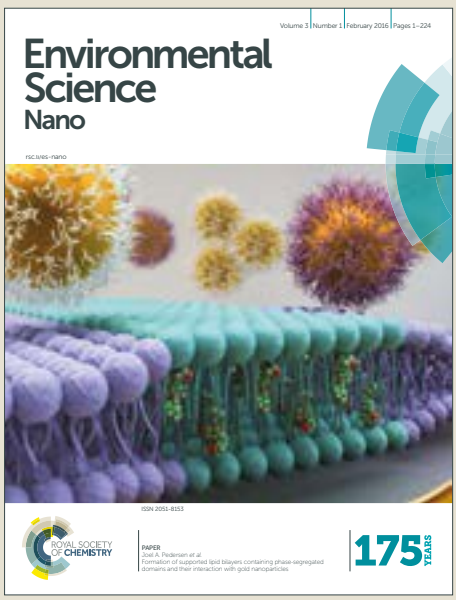

ROYAL SOCIETY OF CHEMISTRY

rsc.li/es-nano

View Article Online
DOI: 10.1039/C8EN00352A

Environmental Significance Statement

Black carbon is known to influence the bioavailability of aromatic hydrocarbons in aquatic ecosystems through adsorption and desorption processes. Much less is known about new ultrathin sheet-like 2D carbon forms in such environments, including their effect on the bioavailability of contaminants to aquatic organisms. This study demonstrates that 2D multilayer graphene nanoplatelets adsorb greater amounts of benzo(a)pyrene than carbon black nanoparticles with similar surface area. This adsorbed benzo(a)pyrene is not bioavailable to a model aquatic invertebrate or to fish liver cells, leading to reduced uptake and response. This study suggests that emerging graphene materials mitigate PAH bioavailability, and at equal surface area are more potent than conventional particle-based carbon forms currently found in sediments.

View Article Online
DOI: 10.1039/C8EN00352A

Impact of emerging, high-production-volume graphene-based materials on the bioavailability of benzo(a)pyrene to brine shrimp and fish liver cells.

Authors: April L Rodd[1]*, Cintia J Castilho[2], Carlos EF Chaparro[3], J Rene Rangel-Mendez[3], Robert H Hurt[2], and Agnes B Kane[1].

Affiliations: [1]Department of Pathology & Laboratory Medicine, Brown University, Providence, RI, 02912. [2]School of Engineering, Brown University, Providence, RI, 02912. [3]Division of Environmental Science, Instituto Potosino de Investigación Científica y Tecnológica, San Luis Potosí, 78216, Mexico.

*** Corresponding Author:** april_rodd@brown.edu

Abstract

With increasing commercialization of high volume, two-dimensional carbon nanomaterials comes a greater likelihood of environmental release. In aquatic environments, black carbon binds contaminants like aromatic hydrocarbons, leading to changes in their uptake, bioavailability, and toxicity. Engineered carbon nanomaterials can also adsorb pollutants onto their carbon surfaces, and nanomaterial physicochemical properties can influence this contaminant interaction. We used 2D graphene nanoplatelets and isometric carbon black nanoparticles to evaluate the influence of particle morphology and surface properties on adsorption and bioavailability of benzo(a)pyrene, a model aromatic hydrocarbon, to brine shrimp *(Artemia franciscana)* and a fish liver cell line (PLHC-1). Acellular adsorption studies show that while high surface area carbon black (P90) was most effective at a given concentration, 2D graphene nanoplatelets (G550) adsorbed more benzo(a)pyrene than carbon black with comparable surface area (M120). In both biological models, co-exposure to nanomaterials lead to reduced bioavailability, with G550 graphene nanoplatelets cause a greater reduction in bioavailability or response than the M120 carbon black nanoparticles. However, on a mass basis the high surface area P90 carbon black was most effective. The trends in bioavailability and adsorption were consistent across all biological and acellular studies, demonstrating the biological relevance of these results in different models of aquatic organisms. While adsorption is limited by surface area, 2D graphene nanoplatelets adsorb more benzo(a)pyrene than carbon black

View Article Online
DOI: 10.1039/C8EN00352A

nanoparticles of similar surface area and charge, demonstrating that both surface area and shape play important roles in the adsorption and bioavailability of benzo(a)pyrene to carbon nanomaterials.

1. Introduction

Engineered carbon nanomaterials are under development or in active commercial deployment in a variety of technologies that range from composite materials, to electrical devices and water filters.[1, 2] Carbon nanomaterials can be fabricated in a range of physical forms that include carbon black nanoparticles (isometric, or "zero" dimensional), carbon nanotubes (one-dimensional) and graphene (two-dimensional sheets). The focus of the present study are 2D carbon nanoforms in the graphene-based material family,[3] some members of which are rapidly emerging as high-volume commercial products with significant exposure potential. The commercial introduction of any new nanomaterial should be accompanied by studies of its potential impacts on human health and the environment, and one aspect of nanomaterial environmental impacts involves material interactions with common environmental contaminants in co-exposure scenarios.[4]

One potential interaction is the adsorption of hydrophobic contaminants like aromatic hydrocarbons from aqueous environments. Polycyclic aromatic hydrocarbons (PAHs) are made up of multiple benzene rings, with or without additional functional groups, and are an important organic pollutant present in aquatic ecosystems. PAHs may enter the environment from petroleum sources or as byproducts of combustion, leading to extensive deposition in both terrestrial and aquatic environments.[5-7] This study focuses on the 5-ring PAH benzo(a)pyrene, which is on the US Environmental Protection Agency's priority pollutant list and a known carcinogen.[8, 9] Like all PAHs, benzo(a)pyrene is a hydrophobic molecule with low solubility in water, driving it to adsorb onto hydrophobic materials suspended in sediment or water and to partition into the lipophilic compartments of an organism or cell.[10, 11] Sediment-bound PAHs can desorb and remain bioavailable to aquatic organisms, particularly those that live in close contact with contaminated sediments.[12, 13] Once within an organism, benzo(a)pyrene is a potent agonist of the aryl hydrocarbon receptor and causes significant induction of xenobiotic metabolism, including cytochrome P450 1A (Cyp1a), and

View Article Online
DOI: 10.1039/C8EN00352A

detoxification enzymes.[14, 15] While benzo(a)pyrene itself is not a mutagen, metabolic activation generates diol-epoxides and quinones that can cause DNA adducts and oxidative stress, leading to cellular damage and toxicity in exposed tissues.[9, 14]

The adsorption of hydrophobic contaminants to particles or aggregates, both natural and engineered, is an important and well-studied phenomenon. In terrestrial environments, soil particles can adsorb hydrophobic materials and sequester them from invertebrates and microbes, and minerals play an important role in the sedimentation of oil in marine environments.[16] Many studies have reported inverse correlations between aromatic hydrocarbon bioavailability and the black carbon content of soils and sediments.[17-20] Black carbon is the generic term for elemental-carbon-based solids in the natural environment that formed through incomplete combustion of biomass or fossil fuels. Black carbon forms include charcoal, formed by solid-state thermal conversion of solid biomass in large-scale fires, and soot particles, formed by gas-to-particle conversion in the flame region of natural fires or engines and subject to atmospheric deposition into soils or sediments. The closest synthetic analogue to charcoal-derived black carbon is activated carbon, which is engineered to have high internal surface area, and has been shown to significantly reduce the bioavailability of adsorbed chemicals.[21] The closest synthetic analogue to soot-derived black carbon is carbon black, which is a manufactured carbon widely used as a pigment, rubber reinforcing agent, and ink.[22] Similar to soot, carbon black is also formed in flames by gas-to-particle conversion and shares its physical structure of primary, equi-axed nanoparticles fused into micron-scale fractal-like aggregates. Previous research has shown that carbon black can adsorb aromatic hydrocarbons from aqueous solution with sufficient affinity to alter the biological response to those hydrocarbons.[21, 23] Both forms of black carbon, and indeed all elemental carbon solids with sp^2-hybridized bonding have a high affinity for adsorption of polycyclic aromatic hydrocarbon (PAH). This adsorption typically occurs through π-π and hydrophobic interactions,[24, 25] and is believed to be the molecular mechanism responsible for reduced bioavailability.

While PAH interactions with black carbon have been widely studied, less is known about the interactions with engineered nanocarbons, especially the emerging 2D forms, which have unique

View Article Online
DOI: 10.1039/C8EN00352A

sheet-like structures and are not yet widely found in the natural environment. While some laboratory studies appear to show reduced bioavailability and protective effects, others show evidence that nanomaterials create an alternate route of uptake and through adsorption/desorption potentiate both uptake and toxicity of the co-exposed molecular toxicant.[26-28] Both the surface chemistry of the nanomaterial and the structure of the aromatic hydrocarbon can influence the strength of this interaction and determine the bioavailability of adsorbed chemicals in different biological media.[29-31] The ionic strength of the aqueous medium can also affect the stability of particle suspensions as well as their interaction with organic pollutants, resulting in differences between freshwater or marine environments.[21]

The present work studies the effects of a model two-dimensional graphene-based material on the bioavailability of and cellular response to a model PAH, benzo(a)pyrene. While monolayer graphene is of interest for certain device applications, much higher production volumes and environmental releases are anticipated for the lower-cost multilayer graphene products fabricated by exfoliation of natural graphite powders, and were thus chosen as the subject of this study. As reference samples, two commercial carbon blacks of widely different primary particle size and surface area were chosen. The carbon blacks serve as models of soot-derived black carbon already found in soils and sediments, and also serve as non-sheet-like reference materials to provide insight into the fundamental differences between traditional carbons and emerging 2D forms. Here three different carbon nanomaterials were used: G550 (a commercial, low-surface-area two-dimensional, multi-layer carbon product marketed as “graphene nanopowder”), P90 (a high-surface-area isometric carbon black), and M120 (a low-surface-area isometric carbon black). The 2D material is a set of ultrathin carbon plates produced commercially by graphite exfoliation, having a surface area of 25 m^2/g, and a mean layer thickness of 23 nm, or 80 layers based on the geometric model relating surface area to layer number, N_L: Surface area (m^2/g) = 2600 / N_L).[32] There is some controversy about the preferred nomenclature for such plate-like materials that are thicker than monolayer graphene, but thinner than conventional (unexfoliated) graphite flakes. These materials have been described by a variety of terms that include “graphene”, “multilayer graphene”, “graphene nanoplatelets (GNPs)”, or “ultrathin

View Article Online
DOI: 10.1039/C8EN00352A

graphite".[3, 33] The use of the single-word phrase "graphene" is not recommended for such materials,[33] but best reserved for the true monolayer. Among the other possibilities, we choose here to use "graphene nanoplatelets (GNPs)", as this has become the most common term used in industry for stiff, plate-like, graphite-derived samples, and is one of the terms listed in the 2017 ISO standard: ISO/TS 80004-13:2017 "Nanotechnologies -- Vocabulary -- Part 13: Graphene and related two-dimensional (2D) materials". Overall, three different carbon nanomaterials were used: G550 (a low-surface-area, two-dimensional, multi-layer (n ~ 80) graphene nanoplatelet sample), P90 (a high surface area carbon black with isometric primary particles), and M120 (a low surface area carbon black with isometric primary particles). While all three materials are composed primarily of sp^2-hybridized elemental carbon, we hypothesized that significant differences in their particle structures and surface chemistries could lead to significant differences in their interactions with PAHs.

To measure the effect of carbon nanomaterials on benzo(a)pyrene bioavailability in different biological systems, two model aquatic organisms were used. As a model planktonic invertebrate, brine shrimp (*Artemia franciscana*) larvae were used to determine the bioavailability of benzo(a)pyrene in these mixtures. In our previous work, brine shrimp larvae were used to determine the effect of carbon black nanoparticles on benzene toxicity.[21] Brine shrimp provide a simple model system for evaluating the potential impact of carbon nanomaterials on planktonic invertebrates in a marine environment. Zooplankton are an important food source for many small fish and other marine organisms, resulting in delivery of bioaccumulated contaminants into the marine food web.[34]

As a complement to the invertebrate assays, the fish liver cell line PLHC-1 was used to assess the cellular response to mixtures. In both fish and mammals, the liver is a sensitive and important target organ for the evaluation of polycyclic aromatic hydrocarbon (PAH) toxicity. As a critical site of xenobiotic metabolism, the liver is responsible for PAH biotransformation and excretion into bile through the expression and activity of metabolic enzymes that determine biological responses.[35] The fish liver cell line PLHC-1 allows us to detect the cellular response to benzo(a)pyrene with high sensitivity using protein and gene expression of the xenobiotic metabolism enzyme primarily responsible for this metabolism, Cyp1a.[36] We also evaluated expression of the transporter Abcc2,

View Article Online
DOI: 10.1039/C8EN00352A

which is responsible for the cellular excretion of compounds like benzo(a)pyrene metabolites and has been reported to be upregulated after PAH exposure.[37, 38] Researchers have previously demonstrated graphene-mediated inhibition of related cellular transporters, potentially increasing co-contaminant toxicity by interfering with cellular excretion of damaging metabolites.[39] By combining the chemical and biological assessments, this paper takes an inclusive approach to the study of the interactions of high volume, two-dimensional graphene nanoplatelets with aromatic hydrocarbons.

2. Materials and Methods

2.1 Materials and Characterization

Three different commercial carbon nanomaterials were used: Printex 90 carbon black (Degussa), M120 carbon black (Cabot), and G550 graphene nanoplatelets ("Graphene Nanopowder 8 nm Flakes" purchased from Graphene Supermarket) (Table 1). Material morphology was characterized using a LEO 1530 field emission scanning electron microscope (SEM) operating at 10 – 20kV or by transmission electron microscopy (TEM) performed using a JEOL 2100F TEM/STEM at an acceleration voltage of 200kV (Figure 1A-D, S1). Before SEM imaging P90 and M120 samples were coated with a layer of AuPd (<1nm). For TEM, all samples were placed on lacey carbon grids. X-ray diffractograms were acquired with a Bruker AXS D8 Advance instrument with Cu Kα radiation (λ = 1.5418 Å) (Figure 1E). Endotoxin concentration in nanomaterial stock solution was evaluated by Associates of Cape Cod, Inc (E Falmouth, MA) with the LAL (Limulus Amebocyte Lysate) gel clot assay. Both M120 and P90 contained 0.62EU/mg and G550 contained 10EU/mg, yielding no more than 0.3EU/mL at the highest tested nanomaterial concentrations, although technical challenges were encountered for the assessment of endotoxin in G550. The zeta potential was evaluated using dynamic light scattering on Malvern Zetasizer Nano – ZS (Figure S1A). Surface area (m^2/g) of the carbon materials was calculated by the Brunauer-Emmett-Teller (BET) theory applied to N_2 adsorption isotherms measured at 77 K using a Quantachrome Autosorb 1 as previously described.[40] Carbonyl, phenolic, lactonic and carboxylic groups of the carbon-based materials were determined by potentiometric titrations using an automatic titrator (Mettler-Toledo T70) as described in previous reports.[41, 42] A series of 2 g/L carbon suspensions were contacted with 25 mL of neutralizing solutions.

View Article Online
DOI: 10.1039/C8EN00352A

The samples were continuously stirred at 125 rpm for 5 days, then titrated with 0.1 N HCl. Dried benzo(a)pyrene was dissolved in dimethylsulfoxide (DMSO) up to a final concentration of 5mg/mL for biological studies and 0.5mg/mL for abiotic adsorption studies, then stored at 4ºC as a stock solution and shielded from light.

2.2 Abiotic Studies of Benzo(a)pyrene Adsorption by Carbon Nanomaterials

Briefly, an aliquot of the benzo(a)pyrene/DMSO stock was diluted with water to achieve 15 ml benzo(a)pyrene solutions/suspensions (0.2 – 10 mg/L) to which 7.5 mg of the test carbon were added to light-shielded glass vials. The carbon loading was fixed at 0.5 mg-C/mL and the final concentration of DMSO never exceeded two percent per volume in all assays. The bottles were shaken in the dark at 120-130 rpm for either 1 or 12hr at 25 °C. At the end of equilibration period (1 or 12hr), the supernatants were separated by centrifugation. The initial pH of the deionized water used for the adsorption study was 6, and for both the 1 hr and 12 hr sample pH was 8 at the end of the equilibration period. The initial and equilibrium concentration of the adsorbate was determined using a Jasco V-760 Spectrophotometer (Jasco OK, USA) at a wavelength of 297.5 nm. The amount of benzo(a)pyrene adsorbed was computed by the mass balance $q_e=V(C_0-C_e)/m$, where C_0 and C_e are the initial and equilibrium concentrations ($mg \cdot L^{-1}$), V is the volume of the solution (L), and m the mass of the adsorbent (g). Experimental values were fitted to Langmuir, Freundlich and Sips adsorption isotherm equations (listed in Table S1) to determine the extent of uptake and further insight into the adsorption mechanisms.

The Langmuir, Freundlich, and Sips models were applied to fit the adsorption data in this study. The Langmuir adsorption isotherm equation assumes a homogeneous energy of adsorption at specific localized sites, resulting in a monolayer with negligible lateral interactions,[43] given by

$$q_e = \frac{Q_{max} b C_e}{1 + b C_e} \qquad (1)$$

Where C_e ($mg \cdot L^{-1}$) and q_e ($mg \cdot g^{-1}$) are the equilibrium concentrations in the liquid and solid phases of the adsorbate, Q_{max} is the monolayer capacity ($mg \cdot g^{-1}$) and b is the Langmuir isotherm

View Article Online
DOI: 10.1039/C8EN00352A

constant ($L \cdot mg^{-1}$). The Freundlich adsorption isotherm implies an exponential distribution of surface sites energies:[44]

$$q_e = K_F C_e^{1/n} \quad (2)$$

Where K_F is the Freundlich isotherm constant ($mg^{1-(1/n)} \cdot L^{1/n} \cdot g^{-1}$) related to adsorption capacity and n is a constant related to the heterogeneity of the adsorption sites.

Finally, the Sips adsorption isotherm equation combines both Langmuir and Freundlich sorption effects. The three-parameter equation is:

$$q_e = \frac{bQ_{max}C_e^{1/n}}{1+bC_e^{1/n}} \quad (6)$$

The Rosenbrook and Quasi-Newton (RQ) methodology was employed to estimate equation parameters using software STATISTICA. The best-fit correlation was selected by the computation of the variance (R^2) parameter and the sum of the squared errors (SSE) (Eq. 7).

$$\sum_{i=1}^{n} \left(q_{e,calc} - q_{e,meas}\right)_i^2 \quad (7)$$

Where $q_{e,calc}$ and $q_{e,meas}$ are the calculated and measured carbon solids concentrations at equilibrium ($mg \cdot g^{-1}$).

2.3 Preparation of Nanomaterials for Biological Exposure

Dry nanomaterial powders were autoclaved at 121ºC for 40 min for sterilization prior to biological assays. To produce suspensions of carbon nanomaterials or carbon nanomaterial mixtures for biological testing, nanomaterials were dispersed in a series of steps (Figure S2). Nanomaterials with and without benzo(a)pyrene were first dispersed in DMSO and mixed with water bath sonication (Branson) for 60 min. For full mixtures, the particles were then diluted with 0.1% BSA in water for a DMSO concentration of 5% and sonicated for 30 min. The concentrated nanomaterial suspensions were then diluted with cell culture media and applied to fish liver cells, or diluted with artificial seawater (Instant Ocean) and applied to brine shrimp. For preparation of separated fractions of the dispersed material, suspensions were centrifuged for 60 min at 13500 rcf at room temperature following the initial 60 min sonication in 100% DMSO. The supernatant was removed to a separate

View Article Online
DOI: 10.1039/C8EN00352A

tube and the pellet resuspended with an equivalent amount of clean DMSO. The two fractions were then diluted to 0.1% BSA + 5% DMSO in water and sonicated for 30 min before dilution into biological media. Suspensions intended for centrifugation were prepared in low-retention microcentrifuge tubes (Axygen) and all others were prepared in glass vials.

2.3 Brine Shrimp Culture and Experimental Methods

Brine shrimp cysts (*Artemia francisca*, INVE) were hatched at room temperature (21ºC +/- 2º) in simulated seawater (Instant Ocean) under continuous light and aeration for 72 hr. Larvae were collected and added to glass vials with exposure medium for 24 hr. Brine shrimp were sacrificed with 10% acetic acid then processed for either fluorescent imaging or histology. For histology, brine shrimp larvae were embedded in agarose and processed for embedding in Technovit 7100 glycol methacrylate using a modified two-step embedding protocol.[45] Brine shrimp were sectioned at 3µm and stained with hematoxylin and eosin for visualization. For fluorescent imaging, larvae were suspended in molten agarose and coverslipped onto a slide. They were imaged with a DAPI filter cube for blue fluorescence using widefield fluorescence and phase contrast brightfield microscopy (Nikon E800). Images were analyzed for quantification of blue fluorescence intensity using CellProfiler software. Results were statistically compared using one-way ANOVA to either the vehicle-treated or benzo(a)pyrene treated controls with Prism 6 software (GraphPad).

2.4 PLHC-1 Fish Liver Cell Culture and Experimental Methods

PLHC-1 cells (ATCC #CRL-2406) in monolayer were maintained in EMEM (ATCC) + 5% fetal calf serum + penicillin and streptomycin (Gibco, 50U/mL each) at 30ºC with CO_2.[36] For all exposures to benzo(a)pyrene, cells were plated in glass vials with or without glass coverslips. Plated cells were directly exposed to treatment media for 24 or 72 hr. Two genes of interest were analyzed using protein (Cyp1a) and gene expression (Cyp1a and Abcc2). For *in situ* detection of Cyp1a protein expression, immunofluorescence was performed as described previously.[36] Samples were counterstained with Hoechst 33342 and imaged using confocal fluorescence and brightfield differential interference contrast (DIC). To pseudocolor nanomaterials in the images, DIC micrographs were inverted and adjusted to emphasize black regions of the original image using ImageJ software.

View Article Online
DOI: 10.1039/C8EN00352A

For quantification of *cyp1a* and *abcc2* gene expression by qRT-PCR, cells were collected for RNA isolation and processed as described previously, with the addition of the *abcc2* primer set (Table S2).[36]

3. Results

3.1 Abiotic B(a)P Adsorption Studies

We hypothesized that adsorption onto carbon surfaces would alter the interactions of benzo(a)pyrene with *Artemia* and fish liver cells, and performed simple experiments in abiotic systems to probe the adsorption process itself. Figure 1 shows adsorption data in the form of isotherm curves for each of the three carbon nanomaterials, after two different contact times (1 hr or 12 hrs). Most of the adsorption was completed after 1 hr (Figure 1F), which is not surprising for these non-porous carbon materials with highly accessible external surface area. The isotherms in the 12 hr data may be reasonably regarded as representing the equilibrium state (Figure 1G). The extent of benzo(a)pyrene adsorption varies significantly with nanocarbon type, and in the rank order P90 > G550 > M120. Some of this trend can be explained by differences in specific surface area, which can be ranked in the order P90 >> G550 ~ M120. To examine the surface area effects in more detail, the adsorption data were fit to the Langmuir, Freundlich, and Sips isotherm models (see Table S1), and the model curves were used to quantitatively compare the fraction surface coverage at a single common point on the isotherm (see Table 2).

Table 2 reports the theoretical benzo(a)pyrene monolayer molar adsorption capacity (mol/m^2) of the different carbons based on their measured BET surface areas and the known geometric area of the benzo(a)pyrene molecular face (255.2 $Å^2$).[46] This estimate assumes that adsorption occurs in parallel, π-π stacking mode as has been previously reported,[47] which is common for higher-MW PAH on carbon surfaces. Table 2 compares the theoretical monolayer adsorption capacity with the experimental value at the equilibrium concentration of 6 mg/L, at which the apparent fractional coverages were estimated. Coverages range from 50-70% for P90 and 50-130% for M120. The outlier

View Article Online
DOI: 10.1039/C8EN00352A

is G550 with apparent monolayer coverages from 160 - 260% (see later discussion). Note that such super-monolayer coverages (> 100%) are not common in the adsorption of fully soluble adsorbates, but are not necessarily surprising in this case, as initial benzo(a)pyrene concentrations used were above saturation for this very poorly water soluble PAH species. Supersaturated solutions can readily form multilayer adsorbed films, or may spontaneously form benzo(a)pyrene oligomers or clusters in suspension that then adsorb or adhere to carbon surfaces to give multilayer deposits.

3.2 Response of Brine Shrimp to CNM Co-exposures

Using the mixing protocol optimized for uptake by biological systems *in vitro*, mixtures were prepared and used to determine bioavailability of benzo(a)pyrene in the presence of these model carbon nanomaterials. Blue fluorescence intensity was used to assess benzo(a)pyrene uptake and generation of metabolites based on their autofluorescent properties (Figure 2). In this mixture benzo(a)pyrene is both adsorbed to the surface of the carbon nanomaterials and as an unbound fraction. Because of the fluorescence-quenching properties of carbon nanomaterials,[40] benzo(a)pyrene that is adsorbed on the nanomaterial surface cannot be directly imaged with this technique. Instead, by targeting a broad spectrum of blue light we can image the autofluorescence of potentially bioavailable benzo(a)pyrene and benzo(a)pyrene metabolites in the brine shrimp larvae. Brine shrimp were exposed to mixtures of benzo(a)pyrene and high surface area isometric carbon black nanoparticles (P90) for 24 hr, then imaged using widefield fluorescence to determine benzo(a)pyrene uptake (Figure 2A). In brine shrimp exposed to mixtures and those exposed to benzo(a)pyrene alone, fluorescence was observed throughout the brine shrimp with the head and cells lining the gut showing the greatest fluorescent intensity. As compared to benzo(a)pyrene exposure alone, increasing doses of isometric carbon black nanoparticles (P90) significantly reduced the amount of visible fluorescence (Figure 2B). These differences in fluorescence intensity were quantified using image analysis (Figure S3).

To determine the distribution of nanomaterials within the organism, brine shrimp were sectioned and prepared for histology (Figure 2A and C). Confirming our phase contrast light microscopy observations, nanomaterials were present only within the gut tract or on the outside of the

View Article Online
DOI: 10.1039/C8EN00352A

brine shrimp exoskeleton, demonstrating that the pattern of blue fluorescence is not directly related to nanomaterial deposition but reflects benzo(a)pyrene uptake by brine shrimp larvae. Image analyses conducted both on whole brine shrimp and with the gut excluded from the analysis demonstrate that the presence of carbon nanomaterial aggregates within the gut does not significantly interfere with the benzo(a)pyrene fluorescence imaging in whole brine shrimp (Figure S4).

Figure 3 shows the effect of 2D graphene nanoplatelets on benzo(a)pyrene bioavailability in comparison to carbon black nanoparticles. Using surface area measurements to normalize concentrations of the three nanomaterials, benzo(a)pyrene uptake was assessed in brine shrimp exposed to the mixtures for 24hr. While the low surface area isometric carbon black nanoparticles (M120) decreased the fluorescence intensity of exposed brine shrimp, they did not decrease fluorescence as much as same relative amount of graphene nanoplatelets (G550) (Figure 3B). All three carbon nanomaterials show the same anatomic distribution within the brine shrimp when examined histologically.

While imaging blue fluorescent intensity allows us to quantify the amount and distribution of benzo(a)pyrene and benzo(a)pyrene metabolites, it does not distinguish between unbound and desorbed benzo(a)pyrene. In exposure to the full mixture, benzo(a)pyrene is present both adsorbed to the nanomaterial surface as well as free in the exposure medium. To determine the possible source of benzo(a)pyrene fluorescence imaged in the brine shrimp, nanomaterial suspensions were prepared with a centrifugation step to separate the nanomaterials from the solvent mixture (Figure S2). Following extensive mixing in DMSO, benzo(a)pyrene and carbon nanomaterial mixtures were centrifuged at high speed to separate the pelleted nanomaterials from the DMSO supernatant. By separating the mixture in DMSO, benzo(a)pyrene remains in solution and does not pellet out after centrifugation (Figure S5). In the nanomaterial mixtures, this separates the pelleted nanomaterial fraction and its adsorbed benzo(a)pyrene from the benzo(a)pyrene that remains freely dissolved in the DMSO supernatant. The pellet and supernatant fractions were then processed for exposure of brine shrimp as with the full mixture. Brine shrimp exposed to any of the pelleted fractions showed no significant fluorescence, indicating no detectable benzo(a)pyrene bioavailability (Figure 4). In contrast,

View Article Online
DOI: 10.1039/C8EN00352A

the supernatant fraction of M120 mixtures showed significant blue fluorescence while the supernatant of G550 did not. The same pattern was observed for P90 mixtures, with fluorescence observed only in the supernatant of the mixtures where benzo(a)pyrene remained bioavailable (Figure S5).

3.3 PLHC-1 Response to Carbon Nanomaterials & Mixtures

Fish liver cells were used to measure the influence of carbon nanomaterials alone on the sublethal response to benzo(a)pyrene measured after exposure to the mixtures. Cells show normal morphology and no significant differences between the three carbon nanomaterials after 24hr exposure to concentrations above those used for mixtures analysis, with rounding observed in cells that have phagocytosed high concentrations of nanomaterials (Figure S6). No significant cell loss or change in nuclear morphology indicative of apoptosis was observed in response to these three nanomaterials alone at the doses used in this study. To determine the effect of the nanomaterials on the genes of interest, cells were exposed to the carbons at high and low concentrations to quantify changes in expression of *cyp1a* and *abcc2* after 24hr exposure (Figure S7). No significant changes were observed in *abcc2* expression after exposure to any of the test carbon nanomaterials. Down-regulation of *cyp1a* was observed at high concentrations of G550 and P90 but all changes remained less than 2-fold, as compared to the >100-fold increase induced by our lowest concentration of benzo(a)pyrene (Figure 5).

To confirm the results of the brine shrimp studies in a vertebrate model system, the fish liver cell line (PLHC-1) was used to evaluate the biological response of cellular exposure to the same mixtures. The response to benzo(a)pyrene was measured using immunofluorescence to detect Cyp1a protein and qRT-PCR to quantify *cyp1a* and *abcc2* gene expression. Using the same relative concentrations of benzo(a)pyrene and carbon nanomaterials used in the brine shrimp study, changes in expression were assessed following exposure to mixtures of nanomaterials and benzo(a)pyrene (Figure 5). A range of P90 carbon black concentrations was mixed with 250ng/mL benzo(a)pyrene to detect dose-dependent changes in *abcc2* and *cyp1a* gene expression after 24hrs (Figure 5A). Compared to benzo(a)pyrene alone, *cyp1a* gene expression exhibits a dose-dependent decrease up to a dose of 15 µg/mL P90, with no further decrease observed at 20 µg/mL. Mixtures with the highest

View Article Online
DOI: 10.1039/C8EN00352A

concentrations (15 and 20μg/mL) of P90 showed a small (less than 2-fold) but statistically significant increase in *abcc2* expression. A dose of 10μg/mL P90 carbon black was identified as decreasing the response to 250ng/mL benzo(a)pyrene and was used to extrapolate the relative surface area needed to change the response to benzo(a)pyrene. Using this surface area to benzo(a)pyrene ratio and a lower concentration of benzo(a)pyrene (50ng/mL), isometric P90 carbon black nanoparticles were compared to mixtures with isometric M120 carbon black and two-dimensional G550 graphene nanoplatelets at the same surface area to assess the effect of the two-dimensional nanoplatelet structure (Figure 5B). While P90 carbon black and G550 nanoplatelets caused a significant reduction in the expression of *cyp1a,* an equivalent amount of M120 carbon black caused no change in the response to benzo(a)pyrene. Neither M120 nor G550 induced changes in the expression of *abcc2* expression*,* and P90 did not cause a change in *abcc2* expression at this lower concentration.

In parallel with the highly sensitive gene expression assays, Cyp1a protein was quantified using immunofluorescence for *in situ* detection of the cellular response to benzo(a)pyrene (Figure 6). Using the same concentrations as in the P90 gene expression assay, P90 demonstrates a dose-dependent decrease in Cyp1a protein (Figure 6A and C). Increased Cyp1a protein was detected in mixtures with 5μg/mL P90, and was reduced to background levels at higher P90 concentrations. Qualitative differences observed in these images were confirmed using image analysis (Figure S8), showing a significant decrease in Cyp1a protein immunofluorescence compared to benzo(a)pyrene alone at P90 concentrations of 10μg/mL and higher. In previous work it was demonstrated that exposure to high, cytotoxic concentrations of benzo(a)pyrene led to decreases in cell number and increased evidence of apoptosis, observed as brightly stained pyknotic and fragmented nuclei.[36] No significant change in cell morphology was observed after exposure to any of the mixtures, with comparable cell densities and nuclear morphology observed in all treatment groups (Figure S10).

To examine the Cyp1a protein response to low surface area M120 carbon black and G550 graphene nanoplatelets, cells were exposed to high concentrations of carbon nanomaterials and benzo(a)pyrene (250ng/mL) for 24hr (Figure 6B and C). Because of the relatively low sensitivity of this assay (Figure S9), concentrations were not matched by surface area and instead, all were exposed to

View Article Online
DOI: 10.1039/C8EN00352A

20μg/mL carbon nanomaterials. When exposed to the full mixture of carbon nanomaterials and benzo(a)pyrene for 24 hr, only P90 significantly reduced Cyp1a protein detected by immunofluorescent labeling. For both M120 carbon black and G550 graphene nanoplatelets, a concentration of 20μg/mL carbon nanomaterial did not significantly reduce Cyp1a protein induction after exposure to 250ng/mL benzo(a)pyrene mixture. While G550 caused a greater reduction than M120, the difference is small and not statistically significant. When exposure time is extended to 72 hr, Cyp1a protein levels are decreased to the level of the vehicle control at 24hr in all groups, indicating no increase in bioavailability over time.

To determine the bioavailability of adsorbed benzo(a)pyrene to the fish liver cells, the mixtures of benzo(a)pyrene and carbon nanomaterials were separated as in the brine shrimp studies (Figure 7). For both the carbon black nanoparticles and graphene nanoplatelets, cells exposed only to the pelleted fraction of the mixture do not show an increase in Cyp1a protein assessed using immunofluorescence labeling after 24hr exposure (Figure 7A). As with the brine shrimp studies, this indicates that the response to benzo(a)pyrene is not primarily associated with the nanomaterials. After 72 hr of exposure, no additional increase in Cyp1a protein expression was observed in cells exposed to carbon nanomaterial mixtures (Figure 7B and C). Instead, the fluorescence intensity of immunolabeled Cyp1a protein remains comparable to vehicle-treated cells, indicating no significant increases in bioavailability over time. Additionally, as with 24 hr exposure no significant alteration in cell or nuclear morphology was observed by confocal fluorescence microscopy after the extended 72 hr exposure (Figure S11).

4. Discussion

This data set provides new information on the behavior of emerging 2D graphene-based materials in complex aquatic environments containing conventional polyaromatic pollutants. The ability of graphene nanoplatelets to mediate PAH bioavailability is compared to nanoparticulate forms of carbon that are models for the soot-derived black carbon currently found in soils and sediments, and for which significant literature data on PAH interactions exist. Using three different carbon nanomaterials, this study specifically evaluates the effect of carbon nanomaterial shape and surface

View Article Online
DOI: 10.1039/C8EN00352A

properties on the adsorption, bioavailability, and response to a model aromatic organic pollutant, benzo(a)pyrene. As a planar polycyclic aromatic hydrocarbon, benzo(a)pyrene has a high affinity for hydrophobic carbon surfaces and will readily adsorb to carbon nanomaterials. Two carbon black nanoparticles, M120 and P90, with different primary particle size and surface area but the same isometric primary particle shape were chosen as models for conventional particulate black carbon. In contrast, the G550 nanoplatelets are thin, two-dimensional flakes of high crystallinity and low oxygen content.

Carbon-based nanomaterials have been used for the removal of different non-polar polycyclic aromatic hydrocarbons (PAH's) such as anthracene, naphthalene, phenanthrene and pyrene.[48, 49] Thus, the two main reported types of adsorption interactions involve a hydrophobic effect or dispersive π-π interactions between the aromatic ring and the π electrons of the graphitic sheets enhanced by nonacidic surface sites. The analysis in Table 1 suggests that graphene-based material's surfaces have an unusually high affinity for benzo(a)pyrene. The materials characterization for the G550 nanoplatelets revealed two exceptional properties of this nanomaterial that may provide an explanation. First, acid-base titrations (Table S3) show that P90 carbon black (2.87 meq/g) and M120 carbon black (2.52 meq/g) have a significantly higher concentration of oxygen-containing functional groups than the G550 (0.94 meq/g). These groups are known to be key determinants of carbon surface chemistry, governing their surface charge and hydrophobicity.[50] The adsorption of uncharged, non-polar organic molecules from aqueous media is believed to occur by hydrophobic interactions and $\pi - \pi$ stacking, and oxygen-containing functional groups create hydrophilic patches that reduce hydrophobic surface area and interrupt the sp^2 π-bonding network.[51] The low oxygen content of G550 favors hydrophobic and $\pi - \pi$ stacking interactions and should contribute to a high benzo(a)pyrene affinity.

Second, the XRD spectrum in Figure 1E shows a similar and low degree of crystalline order for the two carbon blacks, but very high crystallinity for the multi-layer graphene. The high crystallinity is not surprising for this graphite-derived material, which apparently underwent only limited exfoliation to 80-layer thickness, while preserving the graphite atomic structure. The combination of high

View Article Online
DOI: 10.1039/C8EN00352A

crystallinity and flake-like geometry implies that the adsorption sites on multilayer graphene nanoplatelets are primarily extended, flat, graphitic basal planes on the upper and lower flake surfaces, which are low in oxygen content. In contrast, flame-assembled carbon blacks possess smaller, deformed graphene layers with local curvature and higher oxygen content associated with their defect and edge sites. These structural and chemical differences may be sufficient to explain the high affinity of two-dimensional graphene nanoplatelets for benzo(a)pyrene and its high potency in mitigating biological responses.

We evaluated the adsorptive capability of the three carbon nanomaterials using both abiotic chemical assays and aquatic model organisms. For biological studies, dispersion was adjusted to optimize cellular uptake of the material while introducing minimal interfering factors in the adsorption of benzo(a)pyrene to the carbon surfaces. By assembling the mixture in a step-wise manner, benzo(a)pyrene is allowed to first interact with the carbon nanomaterials as a soluble chemical in a protein-free solution, avoiding interference from corona formation or agglomeration with serum and medium components.[52, 53] By first mixing carbon nanomaterials with benzo(a)pyrene in solvent and water, adsorption to the carbon surface occurs before exposure to brine shrimp larvae or liver cells.

To address the possible influence of the nanomaterials on the measured response to benzo(a)pyrene after exposure to the mixtures and pelleted fractions, fish liver cells were used to assess sublethal alterations in gene expression after exposure to the carbon nanomaterials alone. The particle-specific effects on *cyp1a* and *abcc2* expression were limited, with a 2-fold reduction in *cyp1a* the largest observed change. Given the sensitivity of PLHC-1 cells to serum concentrations, we hypothesize that the slight reduction in *cyp1a* gene expression may be due to nanomaterial adsorption of micronutrients from the medium.[40, 54] However, while the downregulation due to G550 nanoplatelets was statistically significant, *cyp1a* expression changes due to nanomaterial exposure were at least one order of magnitude less than the upregulation induced by these mixtures. In contrast, the lowest concentration of benzo(a)pyrene (50ng/mL) induced more than 100-fold increase of *cyp1a*. This suggests that the nanomaterials themselves likely have a limited, if any, inhibitory effect on the molecular response to bioavailable benzo(a)pyrene and that the changes in gene

View Article Online
DOI: 10.1039/C8EN00352A

expression measured in response to mixtures are specifically related to bioavailable benzo(a)pyrene. The effect on Abcc2 function reported in the literature was not observed in this study at the level of gene expression, even after high nanomaterial exposures.[39] This suggests that either the previously described effect on transporter function is due to a post-translational change or that it cannot be extrapolated to other two-dimensional carbon nanomaterials.

Using both imaging of benzo(a)pyrene autofluorescence in brine shrimp and measurement of Cyp1a gene and protein expression in liver cells, we see a dose-dependent reduction in bioavailability of or response to benzo(a)pyrene when added as a mixture with carbon nanomaterials. Using the high surface area P90 isometric carbon black nanoparticles as a reference material, both biological models show reduced uptake of and response to benzo(a)pyrene with increasing nanomaterial concentration. This is likely driven by nanomaterial surface area, and the high surface area material (P90) is most effective on a mass basis.

While other studies have demonstrated potentiation of the response to PAHs by co-exposure to graphene-based materials,[55-57] we observe only a reduction in bioavailability and cellular responses.[26, 58] One of the challenges in comparing different studies is the wide variety of two-dimensional graphene-based nanomaterials and choice reference materials for comparison.[3, 59] Using the same cell line, PLHC-1, and thinner carboxyl graphene, researchers have observed increased cytochrome P450 activity in co-exposure to the aromatic contaminants benzo(k)fluoranthene or β-naphthoflavone.[56] In an *in vivo* model of exposure, co-exposure to a flake-like carbon nanopowder enhanced the uptake of and response to benzo(a)pyrene, leading to increased numbers of apoptotic and necrotic cells.[55] In prior studies like these examples, carbon nanomaterials appear to have a "Trojan-horse" effect where adsorption of the aromatic pollutant leads to enhanced uptake, response, and toxicity.[60] At high concentrations, carbon nanomaterials, including 2D graphene-base materials, can also induce adverse effects that can confound the study of mixtures.[22, 59, 61, 62]

Given the range of physicochemical properties that may influence adsorption of aromatic compounds and uptake of the nanomaterials, we chose two different isometric carbon blacks for comparison with the graphene-based nanoplatelet sample to elucidate the effects of shape and

View Article Online
DOI: 10.1039/C8EN00352A

surface area and focused on sublethal concentrations. When the M120 and G550 nanomaterials were used at comparable surface areas, we detected decreased autofluorescence in the brine shrimp. However, less benzo(a)pyrene uptake was observed in response to the G550 mixtures, suggesting that M120 does not adsorb as much benzo(a)pyrene as the two-dimensional G550 nanoplatelets despite having similar surface area and charge. This is consistent with the acellular adsorption studies and with the more strictly planar geometry and less functionalized surfaces in the graphene nanoplatelet sample than the M120 carbon black sample (see earlier discussion).

Studies with fish liver cells further confirm the contrast between isometric carbon black nanoparticles and two-dimensional graphene nanoplatelets. Focusing on the sublethal response to benzo(a)pyrene exposure in the PLHC-1 cells, we used Cyp1a as a biomarker of benzo(a)pyrene exposure and the cellular response. Cyp1a is a xenobiotic metabolism enzyme and critical component of the detoxification of benzo(a)pyrene and overall adaptive response of the cell.[14, 63, 64] However, in concert with other enzymes this metabolism is also important for the generation of reactive and genotoxic metabolites,[64-66] and some populations of fish have adapted to multi-generational exposure to PAHs and other organic pollutants by reducing their expression of Cyp1a or inducibility of AhR.[67-71] As an indirect measure of the response to benzo(a)pyrene and other aromatic hydrocarbons, changes in Cyp1a expression and activity are widely used as a biomarker of exposure and response to these toxicants in both *in vitro* studies with cells[72, 73] and *in vivo* with field-collected or laboratory-raised organisms.[74-76] Modification of Cyp1a expression and activity can reflect a change in the amount of bioavailable ligand or an alteration in the molecular mechanisms regulating expression and activity.[72, 77-79] In mixtures studies, particularly those with direct interactions between the toxicants, it can be challenging to attribute changes in a given biomarker like Cyp1a to specific molecular mechanisms or to extrapolate results to other mixtures.[60, 80-82] Our results on the changes in the uptake and response to benzo(a)pyrene lay the foundation for future toxicity testing *in vivo* with environmentally relevant model organisms to further elucidate the interaction between biological tissues and mixtures of carbon nanomaterial and aromatic hydrocarbons.[62]

View Article Online
DOI: 10.1039/C8EN00352A

In response to mixtures with carbon nanomaterials and benzo(a)pyrene, Cyp1a gene and protein expression in PLHC-1 cells show a similar pattern of reduced response to benzo(a)pyrene with increasing carbon nanomaterial doses. However, there are important differences between the gene and protein expression endpoints that reflect the conditions used for each assay. At high concentrations of both benzo(a)pyrene (250ng/mL) and carbon nanomaterials (20µg/mL), immunolabeled Cyp1a protein is reduced in a concentration or surface area-dependent manner after 24hr exposure, with only high surface area P90 carbon black significantly reducing the expression of Cyp1a protein. Neither low surface area material, G550 nanoplatelets nor M120 carbon black, significantly decreased Cyp1a protein at this ratio of benzo(a)pyrene to nanomaterials, likely due to their significantly lower surface area compared to P90 carbon black. When the M120 nanoparticles and G550 nanoplatelets were compared quantitatively, the difference in immunofluorescence intensity was small and not statistically significant. In contrast, the fish liver cell gene expression studies were conducted at low concentrations using the effective ratios of nanomaterial surface area to benzo(a)pyrene identified with the brine shrimp. After 24hr exposure to these low-dose mixtures, gene expression of *cyp1a* showed a dramatic difference between isometric M120 carbon black nanoparticles and two-dimensional G550 nanoplatelets. Despite having the same available surface area, M120 carbon black caused no reduction in *cyp1a* gene expression while G550 graphene nanoplatelets reduce it to the level of vehicle-treated cells.

Some of this variation can be attributed to the different relative concentrations and assay sensitivities. The high concentration of benzo(a)pyrene (250ng/mL) used in the cell immunofluorescence study combined with the relatively low available surface area in M120 and G550 leaves a significant amount of unbound benzo(a)pyrene to induce a cellular response. In the gene expression study, a similarly high concentration of G550 and M120 were used to adsorb a much lower amount of benzo(a)pyrene (50ng/mL), allowing the graphene nanoplatelets to more effectively reduce the bioavailability of benzo(a)pyrene. However, the M120 carbon black was unable to significantly reduce the Cyp1a response to benzo(a)pyrene at either concentration in the fish liver cells. In contrast, while it is not as not effective as G550 nanoplatelets, M120 carbon black it is still able to

View Article Online
DOI: 10.1039/C8EN00352A

cause a significant reduction in benzo(a)pyrene bioavailability to brine shrimp following exposure to the complete mixture. A possible explanation may be the different exposure media used for these two biological models. While the mixtures are initially prepared in the same way, the aqueous suspension is then diluted into either a seawater substitute for the brine shrimp or cell culture medium for the fish liver cells. As the benzo(a)pyrene re-equilibrates during the biological exposures, the amount of benzo(a)pyrene adsorbed to the carbon surfaces may change in a media-dependent way.

Both aquatic models were used to determine if adsorbed benzo(a)pyrene was contributing to the response to mixtures. Following the initial mixing of the carbon nanomaterials with benzo(a)pyrene, the mixture was pelleted to separate the carbon nanomaterials from the DMSO solution. By separating the mixture in DMSO, the unbound benzo(a)pyrene remains soluble and is not pelleted with the carbon nanomaterials. In both the brine shrimp and liver cells, the pelleted material caused little to no observable uptake of or response to benzo(a)pyrene after 24 hr, while the supernatant portion induces a significant response comparable to the full unseparated mixture. This demonstrates that the observed benzo(a)pyrene response observed is primarily driven by benzo(a)pyrene that is not associated with the carbon nanomaterials themselves. In fish liver cells, no measurable increase in immunolabeled Cyp1a protein was detected after up to three days of continuous exposure, suggesting that desorption of benzo(a)pyrene may not be a significant factor in the bioavailability of adsorbed materials during extended exposure. When the benzo(a)pyrene control is separated in the same manner, there is no observable precipitate and only the supernatant induces a response. This suggests that by separating the mixture at this step, the pelleted fraction should contain only the nanomaterial-associated benzo(a)pyrene with minimal contamination from the dissolved, unbound portion. Once in the final exposure medium the mixture may re-equilibrate to release benzo(a)pyrene into the medium, but these results suggest that desorption of benzo(a)pyrene is minimal.

Our results also suggest that despite its similarities to the other two nanomaterials, M120 carbon black shows different adsorption kinetics in the various media. As demonstrated in the acellular adsorption studies, G550 graphene nanoplatelets can adsorb more benzo(a)pyrene than

View Article Online
DOI: 10.1039/C8EN00352A

M120 at a given concentration after both 1 and 12hr of equilibration. However, the amount adsorbed increases significantly between 1 and 12hr, with G550 nanoplatelets adsorbing as much as the high surface area P90 at low concentrations. In the biological studies, either the full mixture was used for treatment, or it was separated by removal the nanomaterials by centrifugation after the DMSO mixing step. This limits our observations to the adsorption that occurs in the DMSO phase and does not account for additional adsorption that occurs in the aqueous phase. In the brine shrimp studies, removal of the M120 particles after the DMSO phase of mixing resulted in a much smaller effect on benzo(a)pyrene bioavailability than in an unseparated mixture. This was not true of G550 nanoplatelets or the P90 carbon black. This difference suggests that the affinity of M120 for benzo(a)pyrene in DMSO is not as high as the other nanomaterials, and that further adsorption occurs in the aqueous phase during exposure. This may contribute to the influence of the exposure media for the different biological models and exaggerate differences between the brine shrimp and fish liver cell results.

Interestingly, our gene expression results suggest that there is a limit to how much carbon nanomaterials are capable of reducing the cellular response to benzo(a)pyrene in these mixtures. At P90 carbon black concentrations above 15µg/mL, there is no further reduction in *cyp1a*. Instead, it remains elevated nearly 200-fold above vehicle-treated cells, reduced from the more than 1000-fold increase induced by benzo(a)pyrene alone. With increasing doses, the proportion of adsorbed benzo(a)pyrene should increase, leading to less free benzo(a)pyrene to induce a cellular response. This suggests that the sensitivity of the gene expression assay may be capturing the response to nanomaterial-associated benzo(a)pyrene that has desorbed either before or after cell uptake. In the low dose experiment, similar concentrations of P90 carbon black and G550 graphene nanoplatelets reduced gene expression down to approximately 30-fold above vehicle. While it does not significantly contribute to the response at high concentrations, desorption or a “Trojan horse” mechanism of enhanced uptake may be more important at the lower concentrations used in the highly sensitive gene expression studies and lead to these plateaus. Given that no desorption or increase in bioavailability was observed at the higher concentrations assessed as either a mixture or pelleted

View Article Online
DOI: 10.1039/C8EN00352A

fraction over three days, this emphasizes the importance of testing a wide range of concentrations of adsorbed materials over a longer time period. Further study is needed to understand the changes nanomaterial mixtures undergo during extended exposure in biological and environmental media.

This difference may be exaggerated by the different mechanisms of uptake in our two biological models. In fish liver cells, nanomaterials settle onto the monolayer culture and are internalized by individual cells. Fish liver cells readily take up the small carbon black nanoparticles, but the G550 graphene nanoplatelets tend to form large aggregates and remain outside the cells. The comparatively high cellular uptake of M120 carbon black increases the relative dose per cell. Despite the lack of significant desorption observed in studies with pelleted nanomaterials, the plateau in *cyp1a* reduction seen in the gene expression studies suggest that nanomaterial-associated benzo(a)pyrene can have an impact on cells. In contrast, brine shrimp larvae are primarily ingesting carbon nanomaterial aggregates or being exposed to the aggregates through their exoskeleton. While the cells lining the gut show high levels of fluorescence, our data show no evidence for translocation of carbon nanomaterial aggregates into or across the cells of the gut. Instead, the blue fluorescent signal likely demonstrates the partitioning of benzo(a)pyrene and generation or movement of its metabolites throughout the tissues of the brine shrimp. This suggests that the fluorescence observed in the brine shrimp is not due to benzo(a)pyrene delivered into target or gut cells on the nanomaterial surface. The difference between M120 and G550 mixtures of different ratios in fish liver cells may be due to these different mechanisms of uptake, which do not apply to the free-swimming brine shrimp larvae and the aggregated material they ingest.

Conclusions

This study provides the first data on the biological response of two aquatic model systems to multilayer graphene nanoplatelets, benzo(a)pyrene, and their mixtures. While the acellular evaluation of benzo(a)pyrene adsorption to carbon nanomaterials allows us to predict their interactions in an aqueous environment, assessment of the response in aquatic model organisms connects those results with the nanomaterial's impact on benzo(a)pyrene bioavailability. The graphene-based material is shown to mitigate benzo(a)pyrene uptake into *Artemia franciscana* without causing

View Article Online
DOI: 10.1039/C8EN00352A

damage to the gut lining or altering benzo(a)pyrene distribution within larvae. In the PLHC-1 fish liver cell line, the graphene nanoplatelets significantly reduced the expression of Cyp1a, a biomarker of the cellular response to benzo(a)pyrene exposure. In combining two different biological models, larval brine shrimp and a fish liver cell line, these consistent trends are demonstrated at sublethal nanomaterial exposures across different mechanisms of uptake and endpoints of benzo(a)pyrene bioavailability and response. Abiotic adsorption experiments suggest the ability of graphene to mitigate benzo(a)pyrene bioavailability is due to adsorption on graphene surfaces. Compared to flame-formed carbon nanoparticles used as models for soot-derived black carbon in the environment, the graphene-based materials are more effective at mitigating benzo(a)pyrene bioavailability on a unit surface area basis. We present evidence that this strong antagonistic effect between benzo(a)pyrene and graphene is reflected by graphene's high specific adsorption affinity for benzo(a)pyrene. This, in turn, reflects the low oxygen content and intrinsically planar structure of the flake-like graphene platelets, which creates ideal microenvironments for benzo(a)pyrene adsorption by hydrophobic and π – π surface interactions.

Author Contributions

Carbon nanomaterial characterization and adsorption isotherm measurements were conducted and analyzed by C Castilho and C Chaparro, with assistance in analysis from R Hurt and J Rangel-Mendez. Design of these abiotic experiments was done by C Castilho, C Chaparro, R Hurt and J Rangel-Mendez. A Rodd conducted all biological experiments and analysis, with experimental design by A Rodd and A Kane. A Rodd wrote the initial manuscript in collaboration with A Kane and R Hurt. This study was conceptualized and designed collaboratively by A Rodd, R Hurt, and A Kane.

Conflicts of Interest

There are no conflicts of interest for the authors to declare.

Acknowledgements

We acknowledge financial support from NIEHS Superfund Research Program P42 ES013660. April Rodd also acknowledges an NIEHS Training Grant T32 ES07272 and an IBES Graduate Fellowship from Brown University. The authors extend special thanks to Norma Messier and Dr. Charles Vaslet

View Article Online
DOI: 10.1039/C8EN00352A

for their assistance with RNA isolation and analysis and to Eduardo Sanchez for his assistance with the carbon nanomaterial characterization.

View Article Online
DOI: 10.1039/C8EN00352A

Main paper figures:

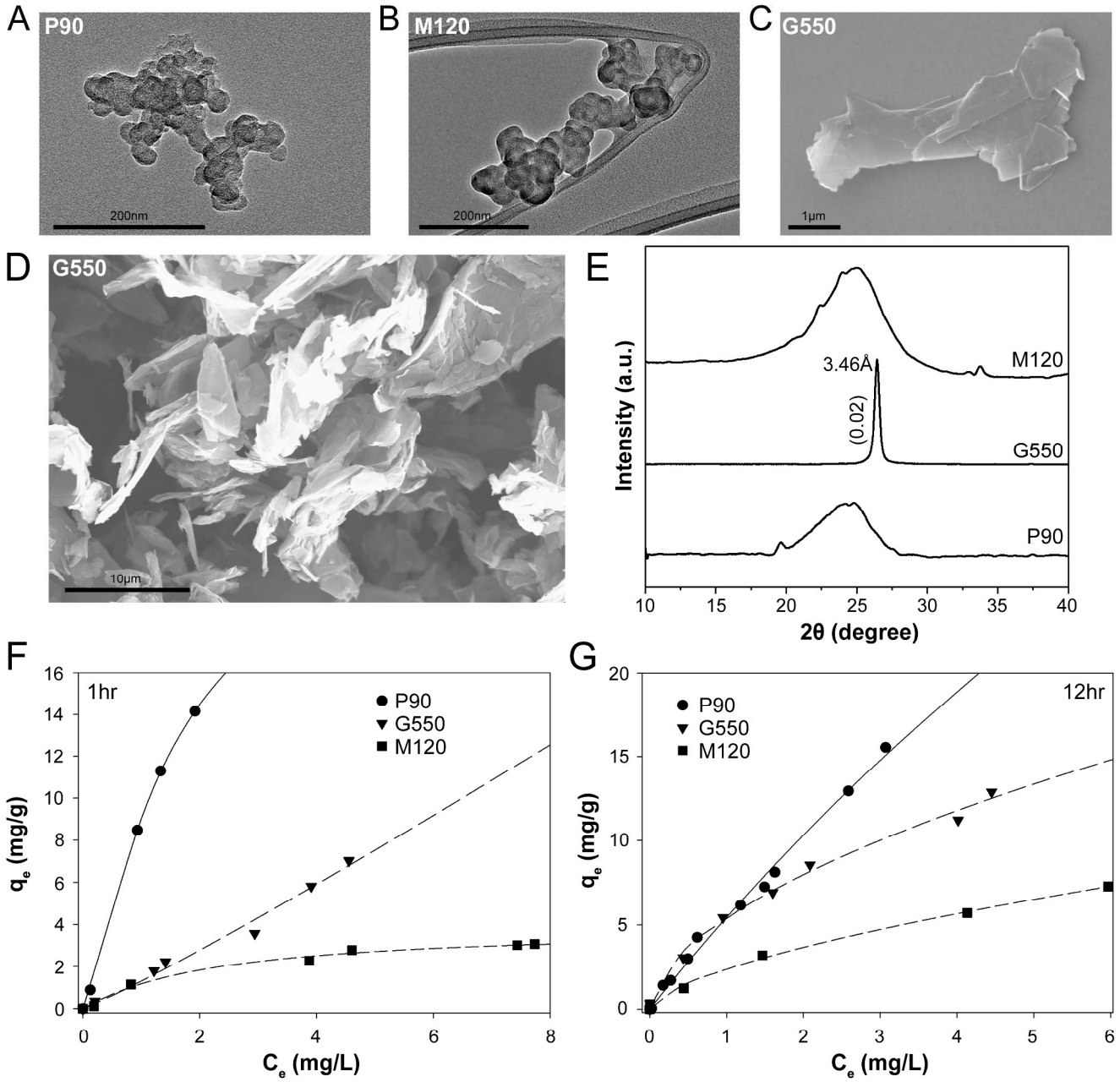

Figure 1: Characterization of carbon nanomaterials and abiotic adsorption data for benzo(a)pyrene. Materials were imaged with TEM for particle size and morphology of P90 carbon black (A) and M120 carbon black (B). G550 graphene nanoplatelets were imaged after dispersion (C) and as a dry powder with SEM (D). E) X-ray diffractogram (XRD) for all three carbon nanomaterials. E) Adsorption isotherms for benzo[a]pyrene on P90, G550 and M120 surfaces with a final sample pH of 8 after 1 hr contact. C_o of benzo(a)pyrene was 10 mg/L at 25 °C. Data fit by Sips equation. C) Adsorption isotherm of benzo[a]pyrene on P90, G550 and M120 surfaces at final pH of 8 after 12 hr equilibration. C_o of BaP was 10 mg/L at 25 °C. Data fit to Sips equation for P90 and 550; M120 data fit to Freundlich model.

View Article Online
DOI: 10.1039/C8EN00352A

Table 1. Nanomaterial properties and characteristics.

	Shape	Supplier	Surface Area (N_2 BET)*	Particle Size
P90 Carbon Black	0D Particle	Degussa	270 m^2/g	15 nm (primary particle)
M120 Carbon Black	0D Particle	Cabot	30 m^2/g	75 nm (primary particle)
G550 Graphene Nanoplatelets	2D Sheet	Graphene Supermarket	25 m^2/g	550 nm (lateral dimension)

* in-house measurements, which differ from the nominal specifications given by the vendor

Table 2. Apparent fractional surface coverage with B(a)P, calculated from the measured adsorption capacity at a equilibrium concentration (C_e) of 6 mg/L.

	1 h			12 h		
Adsorbent	Monolayer coverage Moles/m^2 ($\times 10^{-5}$)[α]	Experimental loading Moles/m^2 ($\times 10^{-5}$)	Apparent fractional surface coverage (%)	Monolayer coverage Moles/m^2 ($\times 10^{-5}$)[α]	Experimental loading Moles/m^2 ($\times 10^{-5}$)	Apparent fractional surface coverage (%)
P90	1.40 X 10^{-4}	7.91 X 10^{-5}	56.6	1.40 X 10^{-4}	9.89 X 10^{-5}	70.7
G550	2.15 X 10^{-5}	3.46 X 10^{-5}	160.8	2.15 X 10^{-5}	5.59 X 10^{-5}	259.6
M120	2.13 X 10^{-5}	1.08 X 10^{-5}	50.8	2.13 X 10^{-5}	2.76 X 10^{-5}	129.6

[α] Theoretical full monolayer coverage from geometry based on a BaP molecular face area of 255.6 $Å^2$.

View Article Online
DOI: 10.1039/C8EN00352A

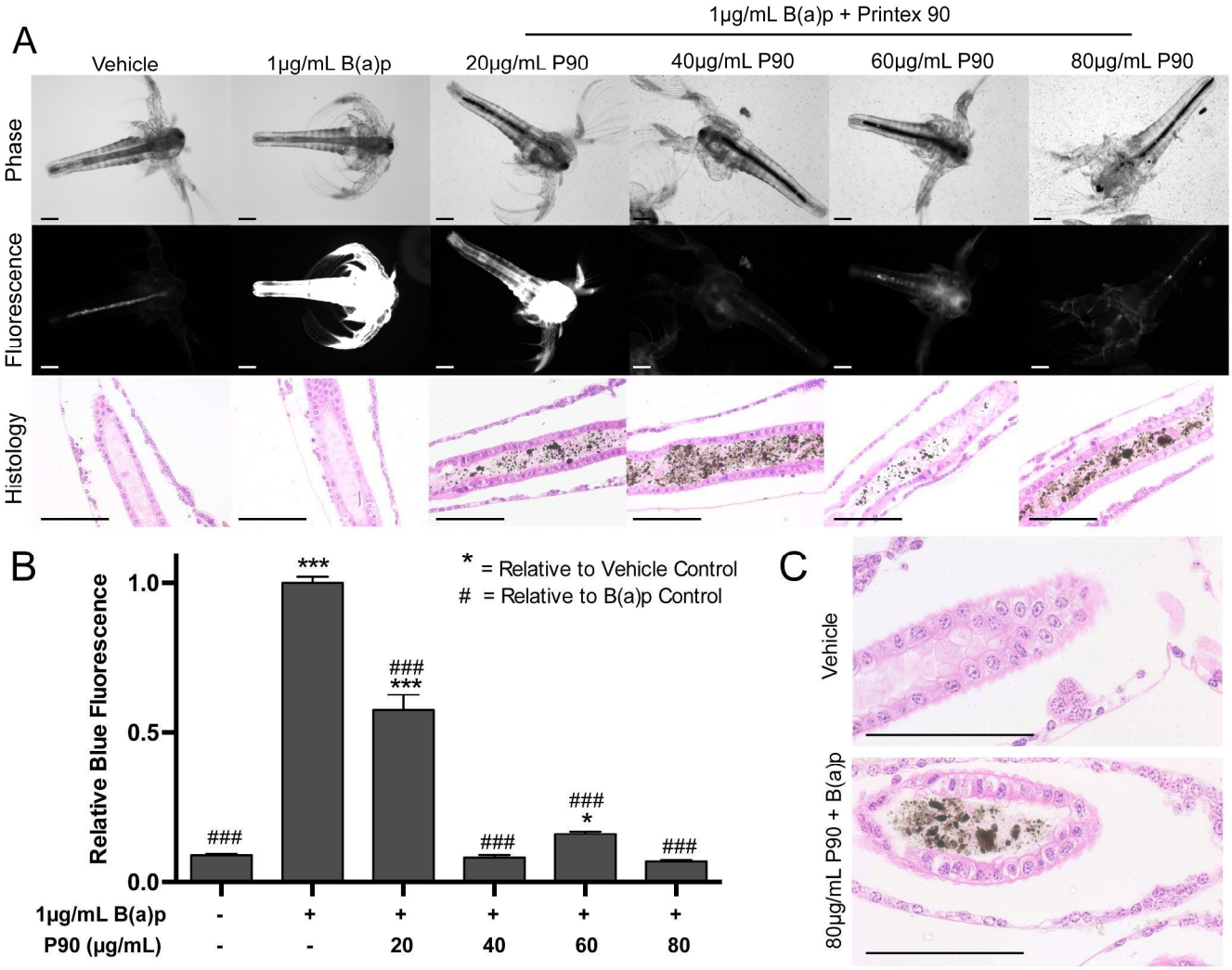

Figure 2: Brine shrimp response to Printex 90 co-exposure. A) Brine shrimp larvae were exposed to 1µg/mL benzo(a)pyrene with or without P90 carbon black for 24 hr, then used for fluorescent imaging or processed for histology. Histological sections stained with hematoxylin and eosin. B) Fluorescent imaging was used in combination with phase contrast for image analysis in CellProfiler to compare fluorescence intensity to vehicle- or benzo(a)pyrene-treated larvae. C) Higher magnification of the histological sections show no sign of cellular uptake of P90 aggregates across the barrier of the gut, and no change in nuclear morphology was noticed after ingestion of 80µg/mL P90 with 1µg/mL benzo(a)pyrene. All fluorescent microscopy settings the same for this figure, with the fluorescence normalized to benzo(a)pyrene-treated brine shrimp for graphing of data. All scale bars 100µm. * or # $p < 0.05$; ** or ## $p < 0.01$; *** or ### $p < 0.001$.

View Article Online
DOI: 10.1039/C8EN00352A

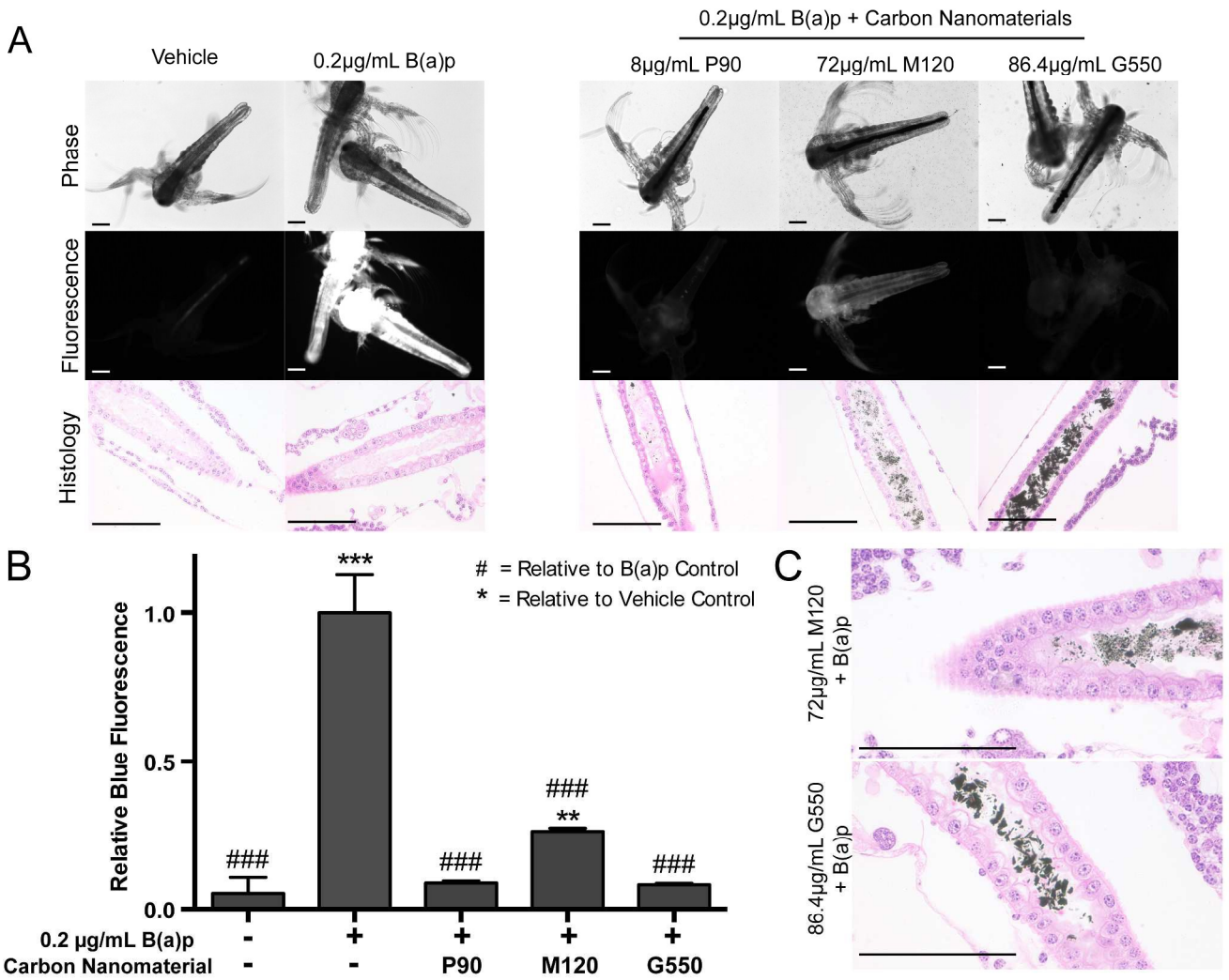

Figure 3: Brine shrimp response to M120 and G550 co-exposure. A) Brine shrimp were exposed to mixtures of P90, M120 or G550 carbon nanomaterials and 0.2µg/mL benzo(a)pyrene for 24hr. To normalize the relative amounts of each nanomaterial, concentrations were chosen to provide the same amount of carbon nanomaterial surface area. After exposure, brine shrimp were imaged for fluorescent microscopy or processed for sectioning and stained with hematoxylin and eosin. B) As with the P90 treated brine shrimp, images were analyzed for fluorescent intensity and compared to vehicle- or benzo(a)pyrene-treated larvae. C) High magnification of the histological sections does not show signs of uptake of either M120 or G550 by the cells lining the brine shrimp gut. All fluorescent microscopy settings were the same for this figure, with the fluorescence normalized to benzo(a)pyrene-treated brine shrimp for graphing of data. All scale bars 100µm. * or # $p < 0.05$; ** or ## $p < 0.01$; *** or ### $p < 0.001$.

View Article Online
DOI: 10.1039/C8EN00352A

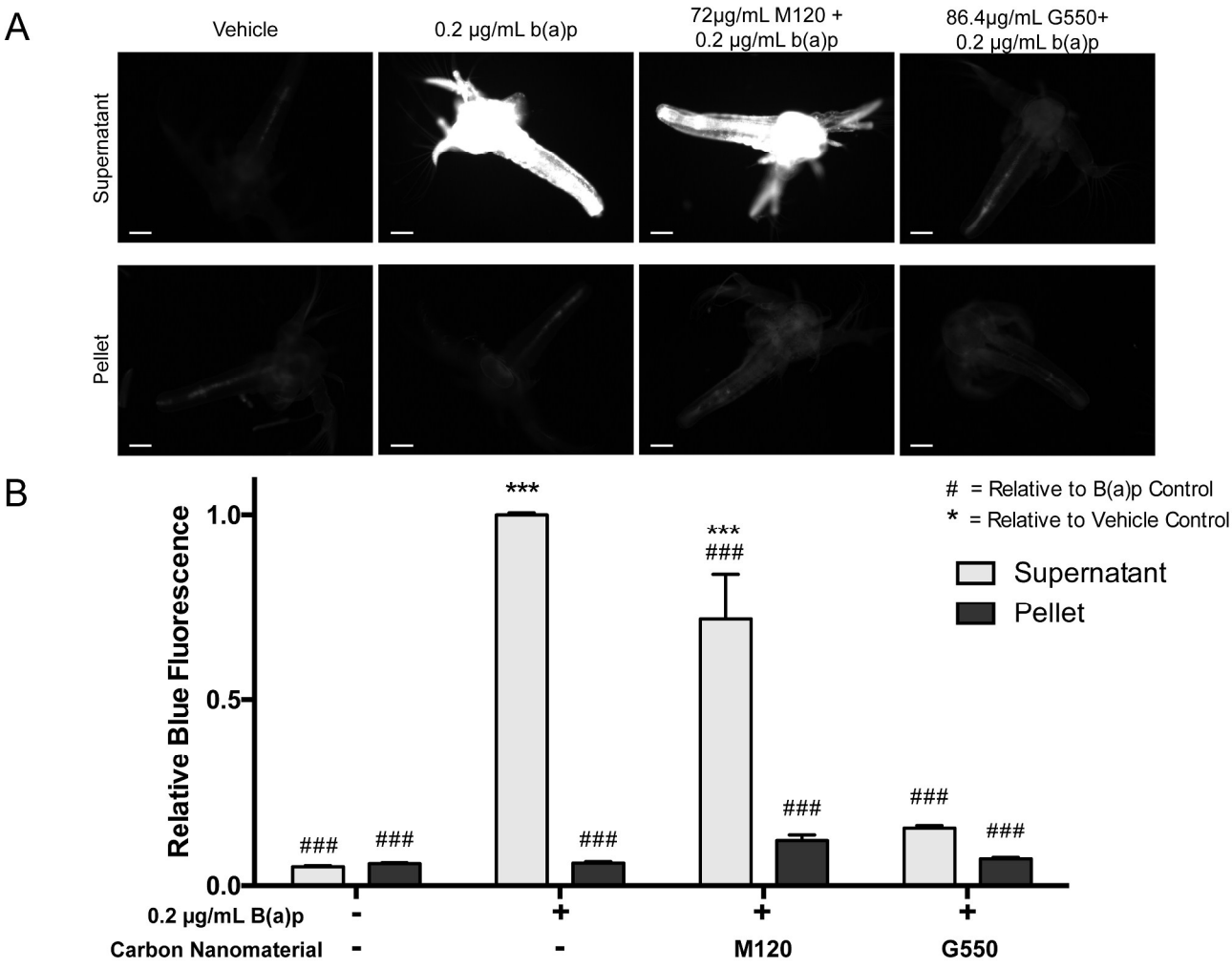

Figure 4: Effects of separated mixture fractions. A) Dispersed carbon nanomaterials and benzo(a)pyrene were separated by centrifugation after 60min of mixing in DMSO. Brine shrimp were then exposed to either the pelleted nanomaterial fraction or the supernatant, which contains any unbound benzo(a)pyrene and imaged for blue fluorescence intensity. B) Image analysis was conducted to compared fluorescence intensity to the supernatant fractions of benzo(a)pyrene- and vehicle-treated larvae. All fluorescent microscopy settings the same for this figure, with the fluorescence normalized to benzo(a)pyrene-treated brine shrimp for graphing of data. All scale bars 100µm. * or # $p < 0.05$; ** or ## $p < 0.01$; *** or ### $p < 0.001$.

View Article Online
DOI: 10.1039/C8EN00352A

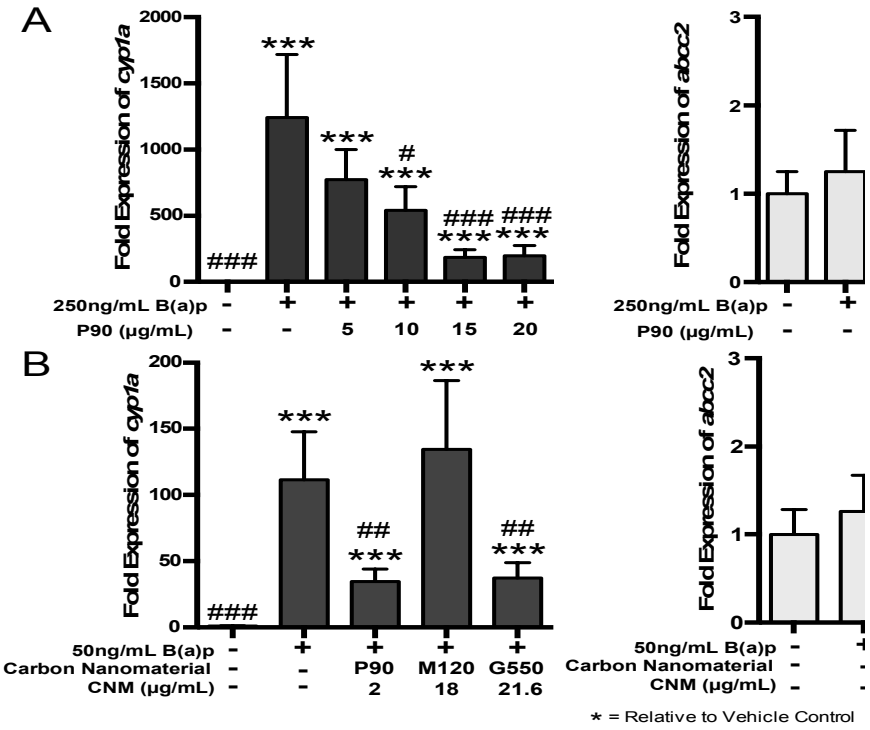

Figure 5: Changes of gene expression in fish liver cells after exposure to mixtures. A) Fish liver cells (PLHC-1 cell line) were exposed to mixtures of 250ng/mL benzo(a)pyrene and increasing P90 carbon black, then assessed for changes in *cyp1a* and *abcc2* gene expression. B) Using the same relative surface areas, fish liver cells were then exposed to 50ng/mL benzo(a)pyrene and P90, M120, or G550 for 24 hr before RNA collection and measurement of *cyp1a* and *abcc2*. All results were compared to the vehicle and benzo(a)pyrene treated groups for each respective experiment. * or # $p < 0.05$; ** or ## $p < 0.01$; *** or ### $p < 0.001$.

View Article Online
DOI: 10.1039/C8EN00352A

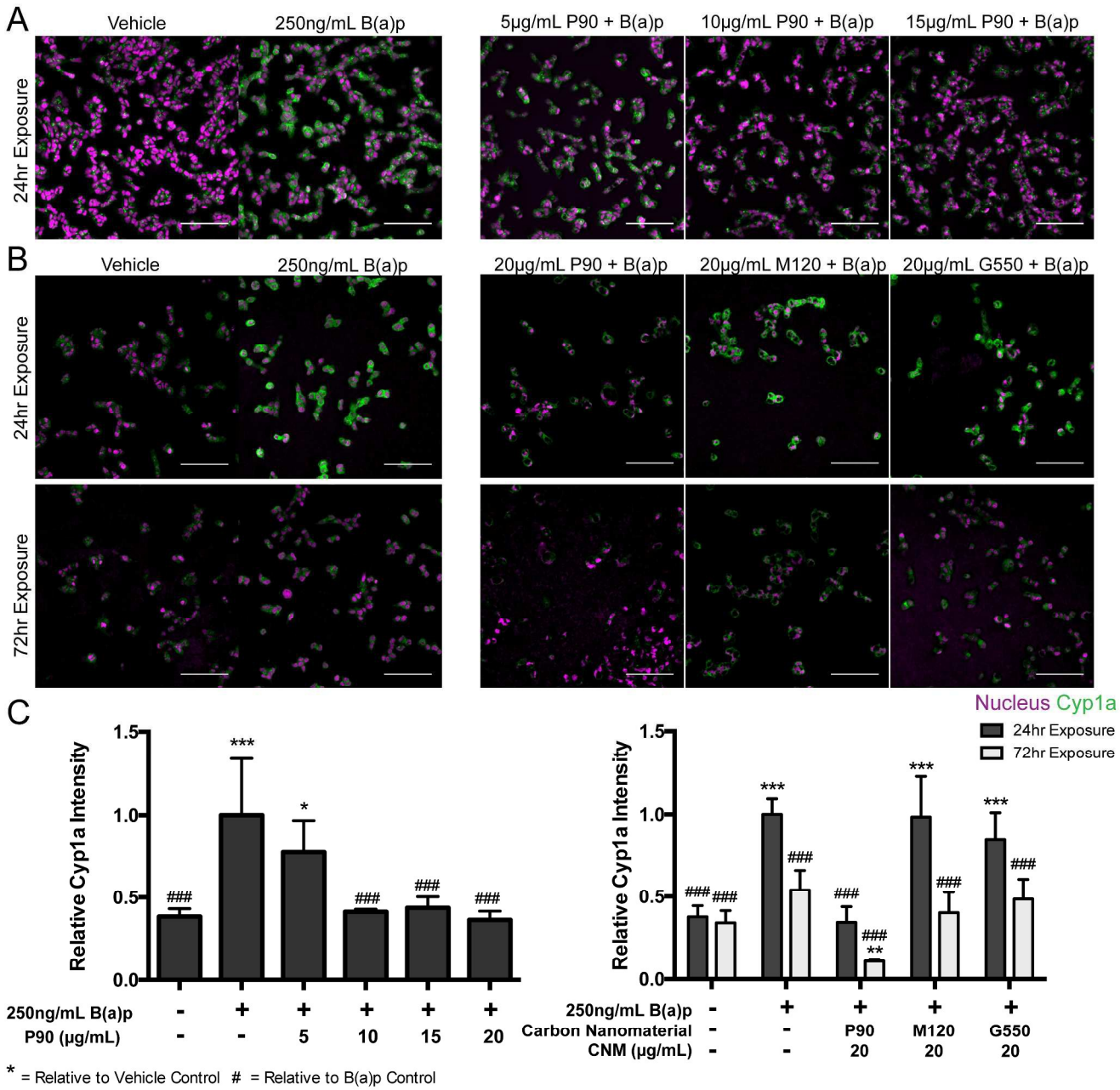

Figure 6: Cyp1a protein response to carbon nanomaterial mixtures. A) Using the same concentrations as the gene expression study, fish liver cells (PLHC-1) were exposed to mixtures of 250ng/mL benzo(a)pyrene and increasing P90 carbon black for 24hr. B) For comparison, cells were also treated with mixtures of 250ng/mL and 20µg/mL P90, M120 or G550 for continuous exposure over 24 or 72hr. Cells from both studies were fixed and processed for Cyp1a immunofluorescence. C) These images were then analyzed for relative immunofluorescence intensity to quantify the effect of carbon nanomaterials on Cyp1a protein expression. * or # $p < 0.05$; ** or ## $p < 0.01$; *** or ### $p < 0.001$.

View Article Online
DOI: 10.1039/C8EN00352A

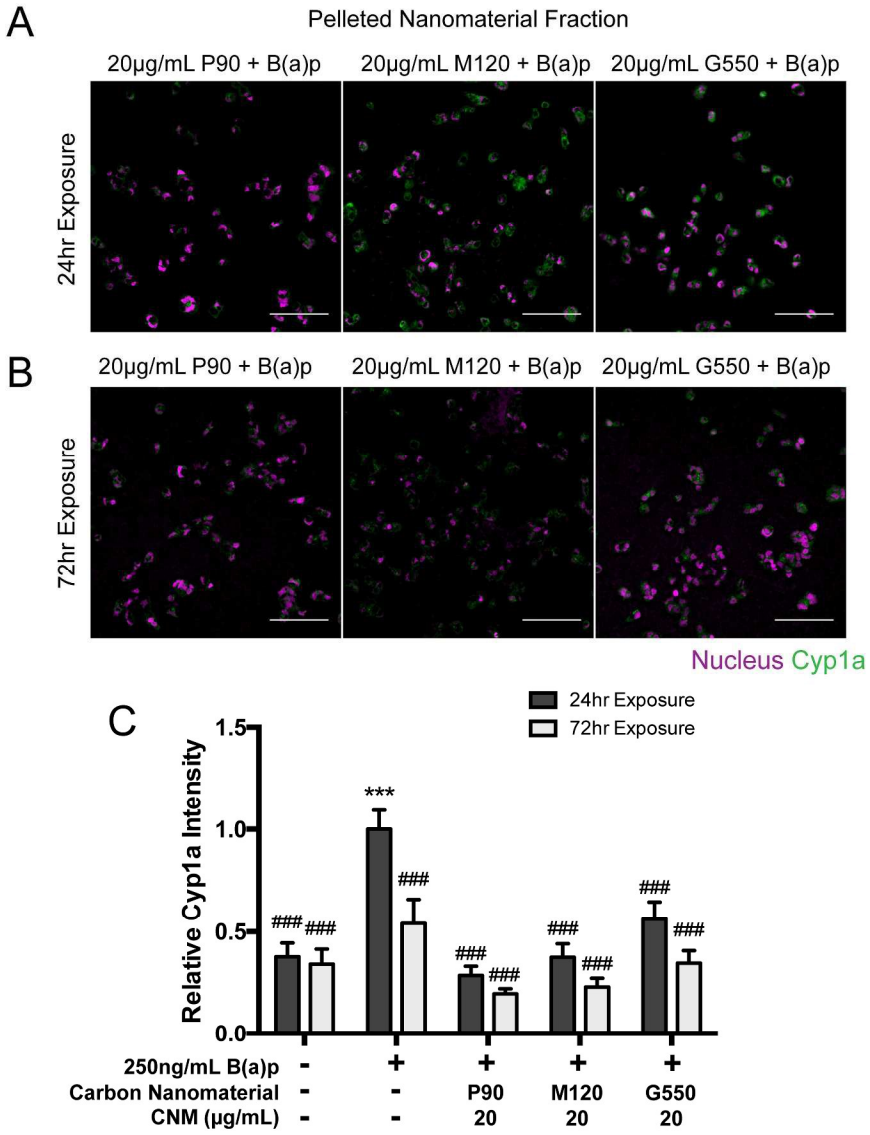

Figure 7: Cyp1a protein response to the pelleted fraction of carbon nanomaterial mixtures. Fish liver cells were treated with the pelleted fraction of mixtures of 250ng/mL and 20µg/mL P90, M120 or G550 for continuous exposure over 24 (A) or 72hr (B). Cells from both studies were fixed and processed for Cyp1a immunofluorescence. C) These images were then analyzed for relative immunofluorescence intensity to quantify the effect of carbon nanomaterials on Cyp1a protein expression. * or # $p < 0.05$; ** or ## $p < 0.01$; *** or ### $p < 0.001$.

View Article Online
DOI: 10.1039/C8EN00352A

References

1. D. Jariwala, V. K. Sangwan, L. J. Lauhon, T. J. Marks and M. C. Hersam, Carbon nanomaterials for electronics, optoelectronics, photovoltaics, and sensing, *Chem. Soc. Rev.*, 2013, **42**, 2824-2860.
2. S. C. Smith and D. F. Rodrigues, Carbon-based nanomaterials for removal of chemical and biological contaminants from water: A review of mechanisms and applications, *Carbon*, 2015, **91**, 122-143.
3. V. C. Sanchez, A. Jachak, R. H. Hurt and A. B. Kane, Biological interactions of graphene-family nanomaterials: an interdisciplinary review, *Chem. Res. Toxicol.*, 2012, **25**, 15-34.
4. S. Pérez, M. la Farré and D. Barceló, Analysis, behavior and ecotoxicity of carbon-based nanomaterials in the aquatic environment, *Trends Analyt. Chem.*, 2009, **28**, 820-832.
5. B. J. Mahler, P. C. Van Metre, J. L. Crane, A. W. Watts, M. Scoggins and E. S. Williams, Coal-tar-based pavement sealcoat and PAHs: implications for the environment, human health, and stormwater management, *Environ. Sci. Technol.*, 2012, **46**, 3039-3045.
6. R. K. Larsen and J. E. Baker, Source apportionment of polycyclic aromatic hydrocarbons in the urban atmosphere: a comparison of three methods, *Environ. Sci. Technol.*, 2003, **37**, 1873-1881.
7. A. R. Johnsen and U. Karlson, Diffuse PAH contamination of surface soils: environmental occurrence, bioavailability, and microbial degradation, *App. Microbiol. Biotechnol.*, 2007, **76**, 533-543.
8. K. Schirmer, D. G. Dixon, B. M. Greenberg and N. C. Bols, Ability of 16 priority PAHs to be directly cytotoxic to a cell line from the rainbow trout gill, *Toxicology*, 1998, **127**, 129-141.
9. A. S. Pastore, M. P. Santacroce, M. Narracci, R. A. Cavallo, M. I. Acquaviva, E. Casalino, M. Colamonaco and G. Crescenzo, Genotoxic damage of benzo[a]pyrene in cultured sea bream (*Sparus aurata* L.) hepatocytes: harmful effects of chronic exposure, *Mar. Environ. Res.*, 2014, **100**, 74-85.
10. C. Andersson, A. Abrahamson, B. Brunström and J. Örberg, Impact of humic substances on EROD activity in gill and liver of three-spined sticklebacks (*Gasterosteus aculeatus*), *Chemosphere*, 2010, **81**, 156-160.
11. R. Barhoumi, Y. Mouneimne, K. S. Ramos, S. H. Safe, T. D. Phillips, V. E. Centonze, C. Ainley, M. S. Gupta and R. C. Burghardt, Analysis of benzo[a]pyrene partitioning and cellular homeostasis in a rat liver cell line, *Toxicol. Sci.*, 2000, **53**, 264-270.
12. S. A. Murawski, W. T. Hogarth, E. B. Peebles and L. Barbeiri, Prevalence of external skin lesions and polycyclic aromatic hydrocarbon concentrations in gulf of mexico fishes, post-Deepwater Horizon, *Trans. Am. Fish. Soc.*, 2014, **143**, 1084-1097.
13. J. C. Bowman, J. L. Zhou and J. W. Readman, Sorption and desorption of benzo(a) pyrene in aquatic systems, *J. Environ. Monit.*, 2002, **4**, 761-766.
14. D. J. Madureira, F. T. Weiss, P. Van Midwoud, D. E. Helbling, S. J. Sturla and K. Schirmer, Systems toxicology approach to understand the kinetics of benzo(a)pyrene uptake, biotransformation, and DNA adduct formation in a liver cell model, *Chem. Res. Toxicol.*, 2014, **27**, 443-453.
15. N. Verma, M. Pink, A. W. Rettenmeier and S. Schmitz-Spanke, Review on proteomic analyses of benzo[a]pyrene toxicity, *Proteomics*, 2012, **12**, 1731-1755.
16. H. Zhang, M. Khatibi, Y. Zheng, K. Lee, Z. Li and J. V. Mullin, Investigation of OMA formation and the effect of minerals, *Mar. Pollut. Bull.*, 2010, **60**, 1433-1441.
17. R. Lohmann, J. K. MacFarlane and P. M. Gschwend, Importance of black carbon to sorption of native PAHs, PCBs, and PCDDs in Boston and New York harbor sediments, *Environ. Sci. Technol.*, 2005, **39**, 141-148.
18. B. Beless, H. S. Rifai and D. F. Rodrigues, Efficacy of carbonaceous materials for sorbing polychlorinated biphenyls from aqueous solution, *Environ. Sci. Technol.*, 2014, **48**, 10372-10379.

View Article Online
DOI: 10.1039/C8EN00352A

19. B. Sundelin, A. K. E. Wiklund, G. Lithner and O. Gustafsson, Evaluation of the role of black carbon in attenuating bioaccumulation of polycyclic aromatic hydrocarbons from field-contaminated sediments, *Environ. Toxicol. Chem.*, 2004, **23**, 2611-2617.
20. S. Pehkonen, J. You, J. Akkanen, J. V. K. Kukkonen and M. J. Lydy, Influence of black carbon and chemical planarity on bioavailability of sediment‐associated contaminants, *Environ. Toxicol. Chem.*, 2010, **29**, 1976-1983.
21. A. L. Rodd, M. A. Creighton, C. A. Vaslet, J. R. Rangel-Mendez, R. H. Hurt and A. B. Kane, Effects of surface-engineered nanoparticle-based dispersants for marine oil spills on the model organism *Artemia franciscana*, *Environ. Sci. Technol.*, 2014, **48**, 6419-6427.
22. WHO IARC Working Group, Carbon black, titanium dioxide, and talc, *IARC monographs on the evaluation of carcinogenic risks to humans*, 2010, **93**, 1-413.
23. K. Lindner, M. Strobele, S. Schlick, S. Webering, A. Jenckel, J. Kopf, O. Danov, K. Sewald, C. Buj, O. Creutzenberg, T. Tillmann, G. Pohlmann, H. Ernst, C. Ziemann, G. Huttmann, H. Heine, H. Bockhorn, T. Hansen, P. Konig and H. Fehrenbach, Biological effects of carbon black nanoparticles are changed by surface coating with polycyclic aromatic hydrocarbons, *Part. Fibre Toxicol.*, 2017, **14**, 8.
24. M. Cao, A. Fu, Z. Wang, J. Liu, N. Kong, X. Zong, H. Liu and J. J. Gooding, Electrochemical and theoretical study of pi–pi stacking interactions between graphitic surfaces and pyrene derivatives, *J. Phys. Chem. C*, 2014, **118**, 2650-2659.
25. C. R. Martinez and B. L. Iverson, Rethinking the term "pi-stacking", *Chemical Science*, 2012, **3**, 2191-2201.
26. J. L. Falconer, C. F. Jones, S. Lu and D. W. Grainger, Carbon nanomaterials rescue phenanthrene toxicity in zebrafish embryo cultures, *Environ. Sci.: Nano*, 2015, **2**, 645-652.
27. J. Lakowicz, M. McNamara and L. Steenson, Particle-mediated membrane uptake of chemical carcinogens studied by fluorescence spectroscopy, *Science*, 1978, **199**, 305-307.
28. T. Lammel and J. M. Navas, Graphene nanoplatelets spontaneously translocate into the cytosol and physically interact with cellular organelles in the fish cell line PLHC-1, *Aquatic Toxicol.*, 2014, **150**, 55-65.
29. A. Rochefort and J. D. Wuest, Interaction of substituted aromatic compounds with graphene, *Langmuir*, 2009, **25**, 210-215.
30. Z. Wang, J. Zhao, L. Song, H. Mashayekhi, B. Chefetz and B. Xing, Adsorption and desorption of phenanthrene on carbon nanotubes in simulated gastrointestinal fluids, *Environ. Sci. Technol.*, 2011, **45**, 6018-6024.
31. E. N. Linard, P. van den Hurk, T. Karanfil, O. G. Apul and S. J. Klaine, Influence of carbon nanotubes on the bioavailability of fluoranthene, *Environ. Toxicol. Chem.*, 2015, **34**, 658-666.
32. F. Guo, M. Creighton, Y. Chen, R. Hurt and I. Kulaots, Porous structures in stacked, crumpled and pillared graphene-based 3D materials, *Carbon*, 2014, **66**, 476-484.
33. A. Bianco, H.-M. Cheng, T. Enoki, Y. Gogotsi, R. H. Hurt, N. Koratkar, T. Kyotani, M. Monthioux, C. R. Park, J. M. D. Tascon and J. Zhang, All in the graphene family – A recommended nomenclature for two-dimensional carbon materials, *Carbon*, 2013, **65**, 1-6.
34. A. Batel, F. Linti, M. Scherer, L. Erdinger and T. Braunbeck, The transfer of benzo[a]pyrene from microplastics to *Artemia* nauplii and further to zebrafish via a trophic food web experiment – CYP1A induction and visual tracking of persistent organic pollutants, *Environ. Toxicol. Chem.*, 2016, 1656-1666.
35. M. Banni, Z. Bouraoui, J. Ghedira, C. Clerandeau, H. Guerbej, J. F. Narbonne and H. Boussetta, Acute effects of benzo[a]pyrene on liver phase I and II enzymes, and DNA damage on sea bream *Sparus aurata*, *Fish Physiol. Biochem.*, 2008, **35**, 293-299.
36. A. L. Rodd, N. J. Messier, C. A. Vaslet and A. B. Kane, A 3D fish liver model for aquatic toxicology: Morphological changes and Cyp1a induction in PLHC-1 microtissues after repeated benzo(a)pyrene exposures, *Aquatic Toxicol.*, 2017, **186**, 134-144.
37. J. Kranz, S. Hessel, J. Aretz, A. Seidel, E. Petzinger, J. Geyer and A. Lampen, The role of the efflux carriers Abcg2 and Abcc2 for the hepatobiliary elimination of benzo[a]pyrene and its metabolites in mice, *Chem. Biol. Interact.*, 2014, **224**, 36-41.

View Article Online
DOI: 10.1039/C8EN00352A

38. S. C. Paetzold, N. W. Ross, R. C. Richards, M. Jones, J. Hellou and S. M. Bard, Up-regulation of hepatic ABCC2, ABCG2, CYP1A1 and GST in multixenobiotic-resistant killifish (*Fundulus heteroclitus*) from the Sydney Tar Ponds, Nova Scotia, Canada, *Mar. Environ. Res.*, 2009, **68**, 37-47.
39. S. Liu, W. Jiang, B. Wu, J. Yu, H. Yu, X.-X. Zhang, C. Torres-Duarte and G. N. Cherr, Low levels of graphene and graphene oxide inhibit cellular xenobiotic defense system mediated by efflux transporters, *Nanotoxicology*, 2016, 1-10.
40. M. A. Creighton, J. R. Rangel-Mendez, J. Huang, A. B. Kane and R. H. Hurt, Graphene-induced adsorptive and optical artifacts during in vitro toxicology assays, *Small*, 2013, **9**, 1921-1927.
41. H. Boehm, Chemical identification of surface groups, *Adv. Catal.*, 1966, **16**, 179-274.
42. E. Toral-Sanchez, J. R. Rangel-Mendez and L. F. Chazaro-Ruiz, Characterization of iron-modified carbon paste electrodes and their application in As(V) detection, *J. App. Electrochem.*, 2016, **46**, 205-215.
43. R. C. Bansal and M. Goyal, *Activated carbon adsorption*, Taylor & Francis, Boca Raton, FL, 2005.
44. H. Freundlich, Über die Adsorption in Lösungen, *Zeitschrift für Physikalische Chemie*, 1907, **57U**.
45. P. K. Kabadi, M. M. Vantangoli, A. L. Rodd, E. Leary, S. J. Madnick, J. R. Morgan, A. Kane and K. Boekelheide, Into the depths: Techniques for in vitro three-dimensional microtissue visualization, *Biotechniques*, 2015, **59**, 279-285.
46. X. Li, S. Shuang, X. Li, L. Kong, L. Xu, P. Tai, X. Lin, C. Jia and Z. Gong, The effect of concentrations and properties of phenanthrene, pyrene, and benzo(a)pyrene on desorption in contaminated soil aged for 1 year, *J. Soils Sediments*, 2013, **13**, 375-382.
47. T. F. Headen, C. A. Howard, N. T. Skipper, M. A. Wilkinson, D. T. Bowron and A. K. Soper, Structure of pi-pi interactions in aromatic liquids, *J Am Chem Soc*, 2010, **132**, 5735-5742.
48. Y. Sun, S. Yang, G. Zhao, Q. Wang and X. Wang, Adsorption of polycyclic aromatic hydrocarbons on graphene oxides and reduced graphene oxides, *Chem. Asian J.*, 2013, **8**, 2755-2761.
49. J. Wang, Z. Chen and B. Chen, Adsorption of polycyclic aromatic hydrocarbons by graphene and graphene oxide nanosheets, *Environ. Sci. Technol.*, 2014, **48**, 4817-4825.
50. C. Moreno-Castilla, Adsorption of organic molecules from aqueous solutions on carbon materials, *Carbon*, 2004, **42**, 83-94.
51. J. Kim, L. J. Cote, F. Kim, W. Yuan, K. R. Shull and J. Huang, Graphene oxide sheets at interfaces, *J. Am. Chem. Soc.*, 2010, **132**, 8180-8186.
52. E. V. Hestermann, J. J. Stegeman and M. E. Hahn, Serum alters the uptake and relative potencies of halogenated aromatic hydrocarbons in cell culture bioassays, *Toxicol. Sci.*, 2000, **53**, 316-325.
53. M. P. Monopoli, C. Aberg, A. Salvati and K. A. Dawson, Biomolecular coronas provide the biological identity of nanosized materials, *Nat. Nanotechnol.*, 2012, **7**, 779-786.
54. E. V. Hestermann, J. J. Stegeman and M. E. Hahn, Serum withdrawal leads to reduced aryl hydrocarbon receptor expression and loss of cytochrome P4501A inducibility in PLHC-1 cells, *Biochem. Pharmacol.*, 2002, **63**, 1405-1414.
55. C. Della Torre, M. Parolini, L. Del Giacco, A. Ghilardi, M. Ascagni, N. Santo, D. Maggioni, S. Magni, L. Madaschi, L. Prosperi, C. La Porta and A. Binelli, Adsorption of B(α)P on carbon nanopowder affects accumulation and toxicity in zebrafish (*Danio rerio*) embryos, *Environ. Sci.: Nano*, 2017, **4**, 1132-1146.
56. T. Lammel, P. Boisseaux and J. M. Navas, Potentiating effect of graphene nanomaterials on aromatic environmental pollutant-induced cytochrome P450 1A expression in the topminnow fish hepatoma cell line PLHC-1, *Environ. Toxicol.*, 2015, **30**, 1192-1204.
57. A. Binelli, L. Del Giacco, N. Santo, L. Bini, S. Magni, M. Parolini, L. Madaschi, A. Ghilardi, D. Maggioni, M. Ascagni, A. Armini, L. Prosperi, C. Landi, C. La Porta and C. Della Torre, Carbon

View Article Online
DOI: 10.1039/C8EN00352A

nanopowder acts as a Trojan-horse for benzo(alpha)pyrene in *Danio rerio* embryos, *Nanotoxicology*, 2017, **11**, 371-381.
58. E. N. Linard, O. G. Apul, T. Karanfil, P. van den Hurk and S. J. Klaine, Bioavailability of carbon nanomaterial-adsorbed polycyclic aromatic hydrocarbons to *Pimphales promelas*: Influence of adsorbate molecular size and configuration, *Environ. Sci. Technol.*, 2017, **51**, 9288-9296.
59. L. De Marchi, C. Pretti, B. Gabriel, P. Marques, R. Freitas and V. Neto, An overview of graphene materials: Properties, applications and toxicity on aquatic environments, *Sci. Total Environ.*, 2018, **631-632**, 1440-1456.
60. S. Naasz, R. Altenburger and D. Kuhnel, Environmental mixtures of nanomaterials and chemicals: The Trojan-horse phenomenon and its relevance for ecotoxicity, *Sci. Total Environ.*, 2018, **635**, 1170-1181.
61. L. Ou, B. Song, H. Liang, J. Liu, X. Feng, B. Deng, T. Sun and L. Shao, Toxicity of graphene-family nanoparticles: a general review of the origins and mechanisms, *Part. Fibre Toxicol.*, 2016, **13**, 57.
62. A. Freixa, V. Acuna, J. Sanchis, M. Farre, D. Barcelo and S. Sabater, Ecotoxicological effects of carbon based nanomaterials in aquatic organisms, *Sci. Total Environ.*, 2018, **619-620**, 328-337.
63. M. S. Denison, A. A. Soshilov, G. He, D. E. DeGroot and B. Zhao, Exactly the same but different: promiscuity and diversity in the molecular mechanisms of action of the aryl hydrocarbon (dioxin) receptor, *Toxicol. Sci.*, 2011, **124**, 1-22.
64. D. W. Nebert and T. P. Dalton, The role of cytochrome P450 enzymes in endogenous signalling pathways and environmental carcinogenesis, *Nat. Rev. Cancer*, 2006, **6**, 947-960.
65. WHO IARC Working Group, Benzo[a]pyrene: Chemical Agents and Related Occupations, *IARC monographs on the evaluation of carcinogenic risks to humans*, 2012, **100F**, 111-144.
66. F. P. Guengerich, Common and uncommon Cytochrome P450 reactions related to metabolism and chemical toxicity, *Chem. Res. Toxicol.*, 2001, **14**, 611-650.
67. R. T. Di Giulio and B. W. Clark, The Elizabeth River story: a case study in evolutionary toxicology, *J. Toxicol. Environ. Health B Crit. Rev.*, 2015, **18**, 259-298.
68. N. M. Reid, D. A. Proestou, B. W. Clark, W. C. Warren, J. K. Colbourne, J. R. Shaw, S. I. Karchner, M. E. Hahn, D. Nacci, M. F. Oleksiak, D. L. Crawford and A. Whitehead, The genomic landscape of rapid repeated evolutionary adaptation to toxic pollution in wild fish, *Science*, 2016, **354**, 1305-1308.
69. A. Whitehead, B. W. Clark, N. M. Reid, M. E. Hahn and D. Nacci, When evolution is the solution to pollution: Key principles, and lessons from rapid repeated adaptation of killifish (*Fundulus heteroclitus*) populations, *Evol. App.*, 2017, **10**, 762-783.
70. P. B. Hamilton, G. Rolshausen, T. M. Uren Webster and C. R. Tyler, Adaptive capabilities and fitness consequences associated with pollution exposure in fish, *Philos. Trans. R. Soc. Lond. B Biol. Sci.*, 2017, **372**.
71. E. M. Oziolor, E. Bigorgne, L. Aguilar, S. Usenko and C. W. Matson, Evolved resistance to PCB- and PAH-induced cardiac teratogenesis, and reduced CYP1A activity in Gulf killifish (*Fundulus grandis*) populations from the Houston Ship Channel, Texas, *Aquatic Toxicol.*, 2014, **150**, 210-219.
72. A. Gabelova, V. Polakova, G. Prochazka, M. Kretova, K. Poloncova, E. Regendova, K. Luciakova and D. Segerback, Sustained induction of cytochrome P4501A1 in human hepatoma cells by co-exposure to benzo[a]pyrene and 7H-dibenzo[c,g]carbazole underlies the synergistic effects on DNA adduct formation, *Toxicol. Appl. Pharmacol.*, 2013, **271**, 1-12.
73. L. Traven, R. Zaja, J. Loncar, T. Smital and V. Micovic, CYP1A induction potential and the concentration of priority pollutants in marine sediment samples--in vitro evaluation using the PLHC-1 fish hepatoma cell line, *Toxicol. in Vitro*, 2008, **22**, 1648-1656.
74. J. J. Whyte, R. E. Jung, C. J. Schmitt and D. E. Tillitt, Ethoxyresorufin-O-deethylase (EROD) activity in fish as a biomarker of chemical exposure, *Crit. Rev. Toxicol.*, 2000, **30**, 347-570.
75. J. Kopecka-Pilarczyk and K. Schirmer, Contribution of hepatic cytochrome CYP1A and metallothionein mRNA abundance to biomonitoring-A case study with European flounder

View Article Online
DOI: 10.1039/C8EN00352A

(*Platichthys flesus*) from the Gulf of Gdansk, *Comp. Biochem. Physiol. C Toxicol. Pharmacol.*, 2016, **188**, 24-29.

76. L. P. Wills, D. Jung, K. Koehrn, S. Zhu, K. L. Willett, D. E. Hinton and R. T. Di Giulio, Comparative chronic liver toxicity of benzo[a]pyrene in two populations of the Atlantic killifish (*Fundulus heteroclitus*) with different exposure histories, *Environ. Health Perspect.*, 2010, **118**, 1376-1381.
77. P. M. Costa, S. Caeiro, C. Vale, T. A. Delvalls and M. H. Costa, Can the integration of multiple biomarkers and sediment geochemistry aid solving the complexity of sediment risk assessment? A case study with a benthic fish, *Environ. Pollut.*, 2012, **161**, 107-120.
78. J. Gräns, J. Johansson, M. Michelová, B. Wassmur, E. Norström, M. Wallin and M. C. Celander, Mixture effects between different azoles and β-naphthoflavone on the CYP1A biomarker in a fish cell line, *Aquatic Toxicol.*, 2015, **164**, 43-51.
79. M. S. Rahman and P. Thomas, Effects of hypoxia exposure on hepatic cytochrome P450 1A (CYP1A) expression in Atlantic croaker: molecular mechanisms of CYP1A down-regulation, *PloS One*, 2012, **7**, e40825.
80. R. P. Schwarzenbach, B. I. Escher, K. Fenner, T. B. Hofstetter, C. A. Johnson, U. von Gunten and B. Wehrli, The challenge of micropollutants in aquatic systems, *Science*, 2006, **313**, 1072-1077.
81. E. Monosson, Chemical mixtures: considering the evolution of toxicology and chemical assessment, *Environ. Health Perspect.*, 2004, **113**, 383-390.
82. F. R. Cassee, J. P. Groten, P. J. van Bladeren and V. J. Feron, Toxicological evaluation and risk assessment of chemical mixtures, *Crit. Rev. Toxicol.*, 2008, **28**, 73-101.

View Article Online
DOI: 10.1039/C8EN00352A

Table of Contents Figure

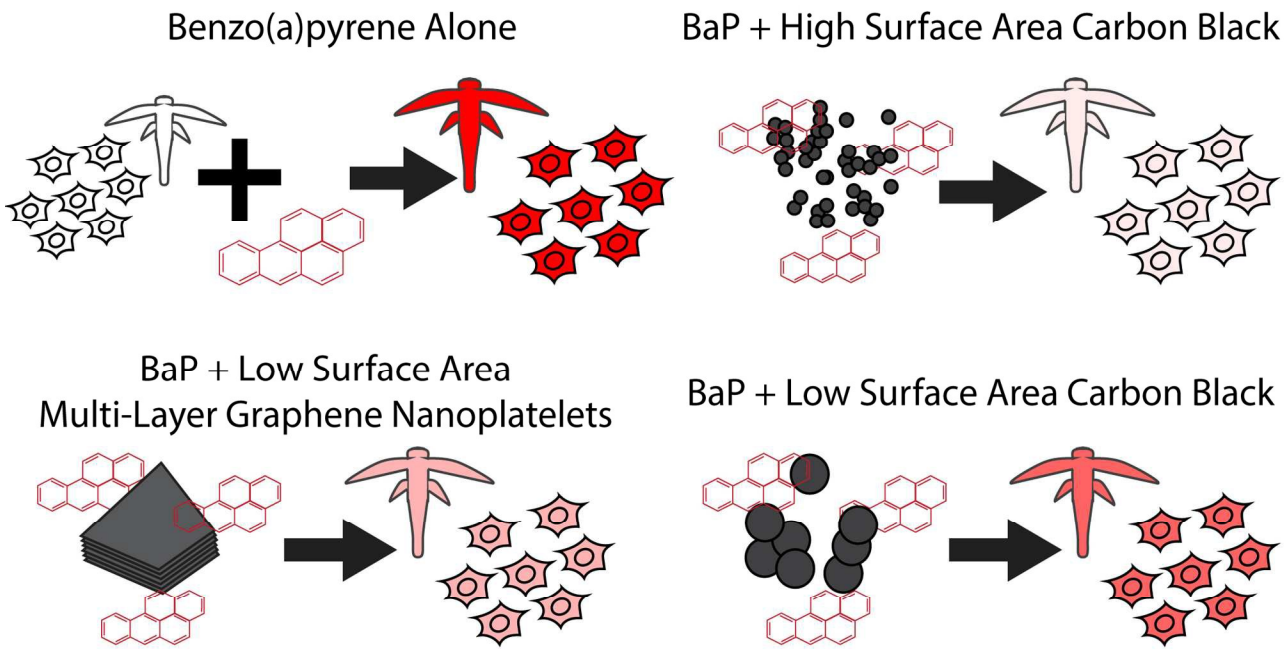

In abiotic measurements, model invertebrates and fish liver cells, multi-layer graphene nanoplatelets reduce benzo(a)pyrene bioavailability more effectively than carbon black nanoparticles of similar surface area.